Coordination Chemistry Reviews 254 (2010) 1135–1150

Contents lists available at ScienceDirect

Coordination Chemistry Reviews

journal homepage: www.elsevier.com/locate/ccr

Review

Electrochemical synthesis and applications of oriented and hierarchically quasi-1D semiconducting nanostructures

Xue-Jun Wu, Feng Zhu, Cheng Mu, Yongqi Liang, Lifen Xu, Qingwei Chen, Ruizhi Chen, Dongsheng Xu*

Beijing National Laboratory for Molecular Sciences, State Key Laboratory for Structural Chemistry of Unstable and Stable Species, College of Chemistry and Molecular Engineering, Peking University, Beijing 100871, PR China

Contents

ARTICLE INFO

Article history:
Received 17 December 2009
Accepted 10 February 2010
Available online 18 February 2010

Keywords:
Semiconductor nanowire array

ABSTRACT

In the last decade, 1D semiconductor nanostructures attracted much attention due to their potential applications in electronics, optoelectronics, sensor, and biotechnology. Among various synthetic strategies, the electrochemical method is a relatively simple and effective way to prepare 1D semiconductor nanostructures. Moreover, electrochemical methods can afford precise processes for controlling the compositions and morphologies of the nanostructured materials. In this review, we present a systematic description of the electrochemical synthesis of oriented and hierarchical quasi-1D semiconducting nanostructures. The main contents containing: (1) electrodeposition of materials in hard porous membranes templates with

Abbreviations: 1D, one dimensional; 2D, two dimensional; VLS, vapor–liquid–solid; SLS, solution–liquid–solid; AAO, anodic aluminum oxide; PM, polymer membranes; DCED, direct-current electrochemical deposition; DMSO, dimethylsulfoxide; ACED, alternating-current electrochemical deposition; TAA, thioacetamide; SCE, standard calomel electrode; HRTEM, high resolution transmission electron microscopy; ED, electrochemical deposition; NW, nanowire; EDA, 1,2-ethylenediamine; CNTs, carbon nanotubes; TNT, TiO_2 nanotube arrays; SEM, scanning electron microscope; ITO, indium tin oxides; SNWs, semiconductor nanowires; XRD, X-ray diffraction; EDX, energy dispersive X-ray; FWHM, full-width at half-maximum; PL, photoluminescence; DSSC, dye-sensitized solar cell; NT, nanotube; NP, nanoparticle; UV, ultraviolet; PSS, polystyrenesulfonate; PAN, polyaniline.

* Corresponding author. Tel.: +86 10 62753580; fax: +86 10 62760360.
E-mail address: dsxu@pku.edu.cn (D. Xu).

0010-8545/$ – see front matter
doi:10.1016/j.ccr.2010.02.014

Template synthesis
Anodic aluminum oxide
Electrodeposition
Electrochemically induced deposition
Sol–gel
Electrophoretic deposition

1D pore geometry or under assistance of the capping reagents for oriented nanowires/nanorods film; (2) multi-step template replication methods, two-step synthetic strategy and anodization methods for uniform nanotube arrays; (3) electrochemical synthetic strategies for complex hierarchical nanostructured films. Additionally, we give a brief introduction about the applications of these quasi-1D semiconducting nanostructures.

1. Introduction

Since the discovery of the carbon nanotube by Iijima in 1991 [1], quasi-one-dimensional (1D) nanostructures including tubes, wires, rods, belts have attracted great attention in the past decade due to their potential application in electronics, optoelectronics, sensor, and biotechnology [2–4]. Because 2D is confined in geometry, 1D nanostructures possess special properties which differ from the corresponding 2D or 3D materials. They represent the smallest dimension structure that can efficiently transport electrical carriers, and thus are used ideally as building blocks to construct a new generation of integrated nanoscale electronic and photonic devices [5–7]. Through the improvement of the methods for preparation of the 1D nanostructures, including vapor–liquid–solid (VLS) [8,9], solution–liquid–solid (SLS) [10], hydrothermal/solvothermal method [11], template-assisted method [12], a variety of 1D nanostructures have been successfully fabricated. Meanwhile, much more complex nanostructures, such heterojunction or co-axis nanowires can also be prepared through elaborate design [13,14], in order to provide optional building blocks for constructing nanodevices. Another issue in the nanodevices from 1D building blocks is the fabrication of blocks with controlled and defined electronic properties. Different from the bulk, this problem is more difficult in 1D nanostructures due to the uncontrollable factors and some disequilibrium steps taking place during the synthesis. So far various single nanodevices, including low temperature single-electron transistors [15,16], field-effect transistors [17,18], intramolecular metal-semiconductor diodes [19,20] and room-temperature ultraviolet lasing [21] have been successfully exploited.

To fulfill the substantial potential applications of the 1D nanostructures in nanotechnology, the assembly of these 1D building blocks, controllably and predictably into 2D or much more complex hierarchically structures is a big challenge. Meanwhile, assembly of 1D nanostructures provides a greater chance to construct more complex nanodevices. Among various hierarchically structures, 1D nanostructure arrays perpendicular to the substrate are of significant interest. Several facile approaches have been used to prepare these types of the nanowires or nanotubes arrays, which have been used as anti-reflection layers [22], superhydrophobic surfaces [23], and lithium ion battery anodes [24]. Due to their special 1D structure which is good for the transport of the electrons, 1D nanostructures arrays, such oxides and sulfides, are good candidates for high performance solar energy cells [25,26].

Among various synthetic strategies, electrochemical synthesis offers a simple and viable alternative to cost-intensive methods such as laser ablation or thermal evaporation synthesis, and is one of the most efficient methods in controlling the growth of 1D semiconductor nanostructures [27]. In particular, it affords precise process control due to its electrical nature, in which the lengths or the aspect ratios and the compositions of the materials can be controlled by the amount of material deposited. This review concentrates on the electrochemical strategies for the synthesis of oriented and hierarchical quasi-1D semiconducting nanostructures. In Section 2 and 3, we will first survey several electrochemical strategies that have been developed for template-assisted synthesis of semiconductor nanowires and nanotubes. Section 4 describes electrochemical synthetic strategies for generating complex hierarchical nanostructured films. In Section 5 we will discuss the structures and the fundamental properties associated with these achieving 1D semiconductor nanostructures, as well as their potential applications in various areas.

2. Oriented nanowire/nanorod films by electrodeposition

2.1. Template-assisted electrochemical synthesis

2.1.1. General

A porous membrane with cylindrical pore geometry can be used as a template for the synthesis of quasi-1D nanostructures. This method was pioneered by Martin [27–30], Moskovits and co-workers [31], and Searson and co-workers [32]. Two types of porous membranes are commonly used: anodic aluminum oxide (AAO) and track-etched polymer membranes. AAO films can be produced upon aluminum metal when aluminum is made the anode in an electrolyte, typically sulfuric, phosphoric, chromic, or oxalic acids at almost any concentration [33–39]. The pore densities as high as 10^{11} pores cm^{-2} can be achieved and the pores in these membranes have little or no tilt with respect to the surface normal resulting in an isolating, non-connecting pore structure, as shown in Fig. 1. Microporous and nanoporous polymer membranes (PM) are commercially available filters, with a broad range of pore diameters (down to 10 nm) and pore densities approaching 10^9 pores cm^{-2}. However, due to the random nature of the pore-production process, the pores in PM are tilted with respect to the surface normal, and a number of pores may actually intersect within the membrane [27].

Among various chemical strategies, electrochemical synthesis in a template is one of the most efficient methods to controlling the growth of a variety of metal [32,40–49], conducting polymer [27,50], oxide and compound semiconductor nanowire arrays [51–96]. As the nanowires grow, the nanopores of the template are filled. Because the nanopores, perpendicular to the AAO membrane surface, are uniform in diameter, and hexagonally packed, the nanowires embedded in the template form highly ordered and vertically aligned nanowire arrays.

2.1.2. Direct-current electrochemical deposition (DCED)

Synthesis of oriented quasi-1D semiconducting nanowire arrays within the pores of the AAO template by DCED involves three steps (Fig. 2) [54]. First, a metal film was deposited by vacuum evaporation or ion sputtering onto the back of the template membrane. Second, semiconductor materials were cathodically deposited on the metal surface at the pore bottom from a solution containing the metal ion (e.g. Cd^{2+}) and another anion (e.g. sulfur and selenium). Finally, the template was chemically dissolved to liberate the nanowires from the pores. The deposition was commonly performed potentiostatically or galvanostatically in a three-electrode configuration. Semiconducting nanowires prepared by DCED were summarized in Table 1.

There are some important considerations in the choice of electrochemical reaction routes and the operational parameters of the DCED method. Contamination of the target material with impurity phases is often a problem with electrodeposition as is the morphological quality of the product. In particular, both the greater

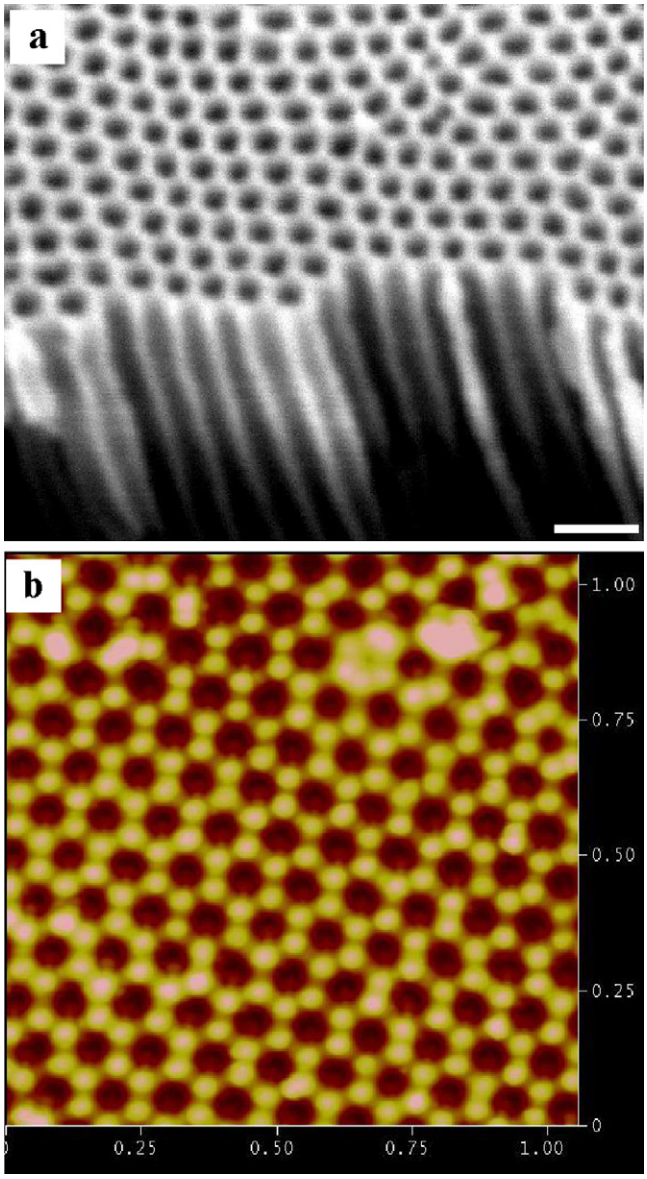

Fig. 1. SEM (a) and AFM (b) micrographs of a 50-nm pore AAO membrane. The scar bar in (a) is 100 nm.

number of active species in the solution and the side reactions render the composition modulation a little trickier. The important point to emphasize is that the electrochemical reaction routes have a key role in the growth of nanowires. Significant improvements have also been claimed in the morphological quality of the resulting nanowires using non-aqueous media [52–62]. For example, highly aligned and crystallized CdS and CdSe nanowires have been prepared by DCED in porous AAO template from dimethylsulfoxide (DMSO) solution containing $CdCl_2$ and S (Se) [52–56]. Also, there have been proponents of the use of non-aqueous solvents. The proclivity of the chalcogen to exist predominantly in low oxidation states in these baths, and the attendant lack of complications in the electrodeposition chemistry have been the principal motivating factors in evaluation of non-aqueous media. For example, CdSe nanowires by DCED in porous AAO template from DMSO solution containing $CdCl_2$ and Se are highly (0 0 2) oriented, and the atomic composition of Cd and Se is very close to a 1:1 stoichiometry [56]. However, in $CdCl_2$ and SeO_2 ammonia alkaline solutions, the deposited nanowires are randomly oriented and the ratio of Se to Cd depends on the pH of the deposition bath [63,64]. Another important factor is that interference from solvent electrochemistry is circumvented in aprotic media; this proves to be crucial in the electrodeposition synthesis of relatively difficult systems such as ZnX (S, Se, Te).

An attractive feature of the electrochemical synthesis approach is the ease with which alloy nanowires may be generated. Composition modulated II–VI and III–V based semiconductors are now widely used to fabricate the superlattices and heterojunction bipolar transistors with a 2D film configuration [97]. Similar to the ideas in 2D counterpart, designed energy-band engineering of nanowires is expected to yield nanoscale devices with interesting properties and functions. Xu and co-workers present a class of alloyed II–VI semiconductor-ternary $CdS_{1-x}Se_x$ nanowires by DCED, in which the ratio of S to Se in the nanowires was controlled by adjusting the relative amounts of the starting materials [79]. These alloyed $CdS_{1-x}Se_x$ nanowires are highly crystalline, and no phase-separate Cd was found. Optical measurements indicate that band gaps of these well-structured nanowires are continuously tuned from 1.7 eV (CdSe) to 2.4 eV (CdS). In addition, other ternary compound nanowires, such as $Ag_{2+\delta}Se_{1-x}Te_x$ [59], $Bi_2Te_{3-y}Se_y$ [80], and $Bi_{2-x}Sb_xTe_3$ [81], have also been prepared by this DCED method.

2.1.3. Alternating-current electrochemical deposition (ACED)

The compact barrier layer between the porous AAO and Al substrate obstructs the passage of direct current. Thus, it is difficult to directly deposit materials on the AAO/Al substrate by DCED. Routkevitch et al. demonstrated that the rectifying properties of the oxide barrier layer that separates the bottom of the pores from the underlying aluminum substrate make it possible to use ACED method [31]. In the case of ac electrolysis of CdS nanowires, 30–50 V AC (60–500 Hz) was applied between the Al/AAO working electrode and a graphite counter electrode. The deposited CdS nanowires are mainly hexagonal CdS with *c*-axis preferentially oriented along the length of the pore. Other semiconductor nanowires, such as CdSe, $Cd_xZn_{1-x}S$, CdS_xSe_{1-x}, and GaAs, have also been fabricated by this strategy [75].

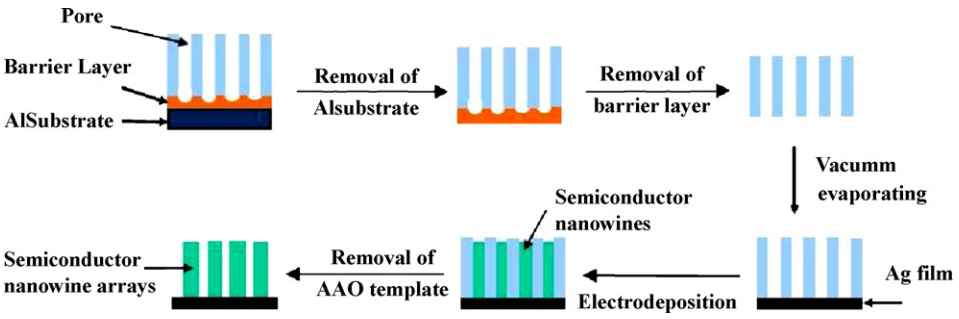

Fig. 2. DC electrochemical synthesis scheme. Adopted from [54]. ©IUPAC (2000).

Table 1
Semiconducting nanowires of various materials prepared by DCED.

Compound	Electrolyte	Solvent	Technique[a]	T	Ref(s)
CdS	$CdCl_2$, S	DMSO	G	110 °C	[53–55]
CdS	$CdSO_4$, EDTA,$Na_2S_2O_3$	Water	G	R.T.	[54]
Ag_2S	$AgNO_3$, S	DMSO	P	120 °C	[60]
Bi_2S_3	$BiCl_3$, S	DMSO	P	120 °C	[61]
CdSe	$CdCl_2$, Se	DMSO	G	185 °C	[54,56]
CdSe	$CdCl_2$, SeO_2,Na_2SO_4,NH_3	Water	P	R.T.	[63]
CdSe	$CdSO_4$, H_2SeO_3, Na_2SO_4	Water	P	R.T.	[64]
PbSe	$Pb(NO_3)_2$, H_2SeO_3,EDTA	Water	P	R.T.	[62]
Ag_2Se	KSCN, $AgNO_3$, KNO_3, SeO_2	Water	P	R.T.	[65]
Ag_2Se	$NaNO_3$, $AgNO_3$, $SeCl_4$	DMSO	P	65 °C	[59]
Ag_2Se	$AgNO_3$ + SeO_2, H_2SO_4	Water	P + G	R.T.	[66]
CdTe	$CdCl_2$, $TeCl_4$, KI	EG	P	160–175 °C	[57]
Ag_2Te	$NaNO_3$, $AgNO_3$, $TeCl_4$	DMSO	P	80 ± 1 °C	[58]
Bi_2Te_3	Te, Bi, HNO_3	Water	G	R.T.	[67–69]
Bi_2Te_3	$Bi(NO_3)_3$, Te, HNO_3	Water	G	R.T.	[51,70]
ZnO	$Zn(NO_3)_2$	Water	P	70 °C	[71]
MnO_2	$MnSO_4$, $(NH_4)_2SO_4$	Water	G	R.T.	[72]
V_2O_5	$VOSO_4$, H_2SO_4	Water	P	R.T.	[73]
Cu/Cu_2O	$CuSO_4$, Lactic acid, NaOH	Water	G	R.T.	[74]
CdS_xSe_{1-x}	$CdCl_2$, S, Se	DMSO	G	160 °C	[79]
$Ag_{2+\delta}Se_{1-x}Te_x$	$CdCl_2$, $SeCl_4$ and $TeCl_4$	DMSO	P	65 °C	[59]
$Bi_2Te_{3-y}Se_y$	Bi, Te, Se, HNO_3	Water	P	25 °C	[80]
$Bi_{2-x}Sb_xTe_3$	Bi, Te, HNO_3, $SbCl_3$, Tartaric acid	Water	P	R.T.	[81]

[a] *Abbreviations*: P, potentiostatic; G, galvanostatic.

ACED is a simple method to fabricate aligned nanowires in AAO template while retaining the compact barrier layer [31]. A major disadvantage of this synthesis route is that there are large numbers of stacking faults and twinned segments in the deposited nanowire and the structure of the nanowire appears to be mainly the hexagonal form, interleaved with domains of cubic structure [78]. In general, for the case of electrodepositing in the pore of the AAO templates, the diffusion direction is limited to one dimension. The diffusing rate may be much slower than the surface electrochemical reaction and the diffusing process would limit the nanowire growth. For ac process, the rate and the direction of the diffusion would vary with the alternation of the electric field, and thus make a high density of defects and small polycrystalline CdS structure in the nanowires [31,78].

2.1.4. Electrochemically induced deposition

Direct electrochemical deposition can afford precise process control and enables good control over stoichiometry. However, both the greater number of active species in the solution and the side reactions render the composition modulation a little trickier. The deposition of the nanowires controlled by electrochemical reaction usually results in a polycrystalline structure. These problems should be avoided if the deposition is controlled by a chemical reaction rather than by the electrode kinetics.

Xu and co-workers have reported an electrochemically induced deposition method to prepare CdS single-crystal nanowires from an acidic chemical bath containing 0.05 M $CdCl_2$ and 0.10 M thioacetamide (TAA) [82]. This process involves electroreduction of protons on conductive substrates and chemical bath deposition of materials on the electrode/solution interface in the pores of the template. The component processes may be represented by the following equations:

$$2H_2O + 2e = 2OH^- + H_2 \quad (1)$$

$$CH_3CSNH_2 + 2OH^- = CH_3COONH_4 + S^{2-} \quad (2)$$

$$S^{2-} + Cd^{2+} = CdS \quad (3)$$

The deposition of CdS was performed potentiostatically at a potential value of −0.65 V (vs. SCE) in a three-electrode configuration in a glass cell at 70 °C. After deposition in 20 nm AAO template for 8 h, the length of the nanowire is up to 10 μm, while the nanowires with 2–3 μm lengths are found in 90 nm template. HRTEM images reveal that these nanowires have a uniform hexagonal CdS single-crystal structure (Fig. 3a and b). Single-crystal nanowires with diameter small than 5 nm have also been prepared.

This method differs from direct ED in that the deposition does not involve reduction of Cd^{2+} or TAA but requires the reduction of the protons at a low current density. The electroreduction of protons imposes a pH gradient at the vicinity of the substrate to reduce the activation barrier for the hydrolysis of TAA. In this case, the CdS nanowire growth is not controlled by the electrode kinetics and not disturbed by the reactions in the solution phase. Therefore, this method allows us to deposit single-crystal CdS nanowires. Of course, the same approach may be valid also in the deposition of other metal sulfide single-crystal nanowires.

2.1.5. Sol–gel electrophoretic deposition

Sol–gel chemistry has evolved into a general and powerful approach for preparing inorganic materials. This method typically entails hydrolysis of a solution of a precursor molecule to obtain first a suspension of colloidal particles (the sol) and then a gel composed of aggregated sol particles. The gel is then thermally treated to yield the desired material. This approach for the synthesis of inorganic materials has advantages in the preparation of both high-purity materials at a lower temperature and homogenous multi-component systems by mixing precursor solutions. Martin's group first conducted sol–gel synthesis within the pores of the AAO template to create both fibrils and tubules of the desired material, using a simple immersion method [98,99]. They found that whether tubules or fibrils are obtained is determined by the immersion time, the temperature of the sol and the electric properties of the pore walls. By this method, nanostructures (nanowires and nanotubules) of a variety of oxides, complex oxide materials [98–104], and other semiconductors have been synthesized [105]. However, there are some potential limitations to this technique. For example, since the only driving force of this technique is capillary action, for the sol with higher concentration, the filling of the pores would be difficult (at the same time destabilization of the sol remain a big problem), but low concentration leads to nanomaterials with serious shrinkage and cracking.

Sol–gel electrophoretic growth of nanowires by Cao and coworkers throws some light on overcoming the limitations of the

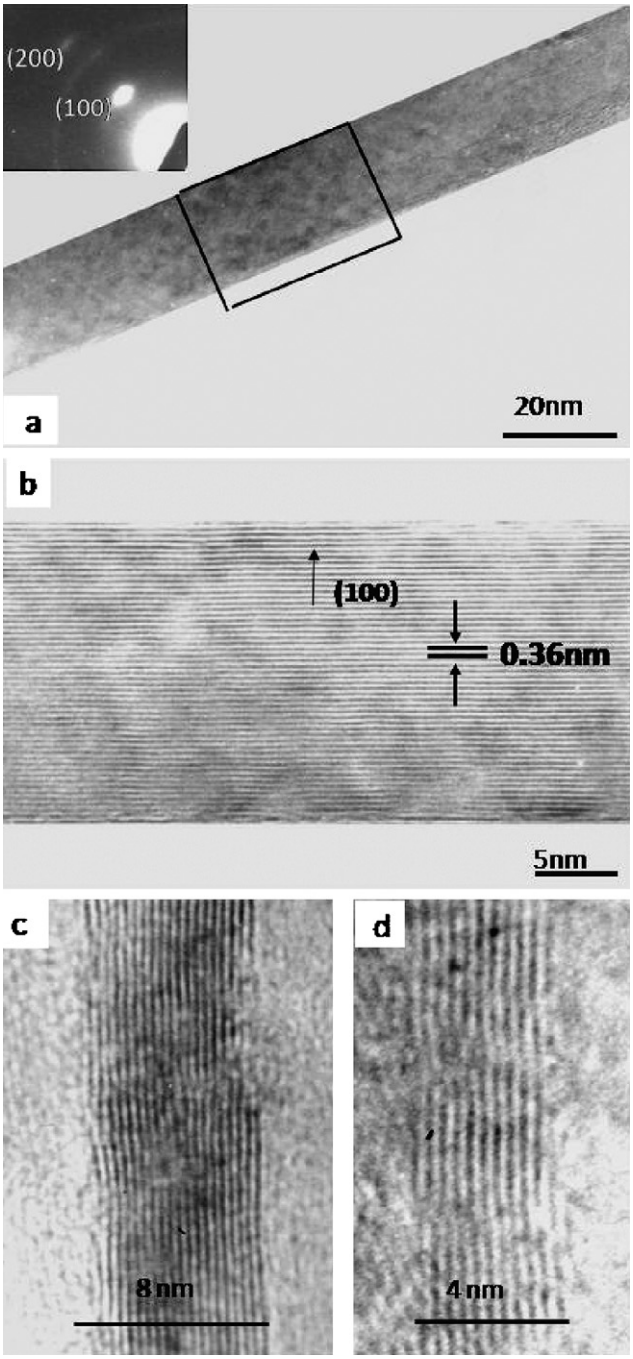

Fig. 3. TEM (a) and HRTEM (b–d) images of individual nanowires with different diameters of: (a and b) 20 nm, (c) 8 nm, and (d) 4 nm. The inset in (a) is the electron diffraction pattern taken from the single nanowire. Adopted from [82]. ©John-Wiley (2000).

direct sol filling method [83,84]. First, a proper sol contains solid nanoclusters of the desired stoichiometric chemical composition. If the sol is electrostatically stabilized, then the charged nanoclusters will have an oriented diffusion, parallel to the field direction, when an electric field is applied to the sol. While using this sol–gel electrophoresis in the template-assisted growth of nanorods, an electric field was applied to draw the charged sol nanoclusters into the template pores. For positively charged sol particles, an anode of Pt mesh is immersed in the sol, and the cathode used is aluminum. For negatively charged sol particles, the electrodes are reversed. The PC membrane is attached to the electrode with a piece of double-sided conductive tape, to provide a conductive path from the membrane

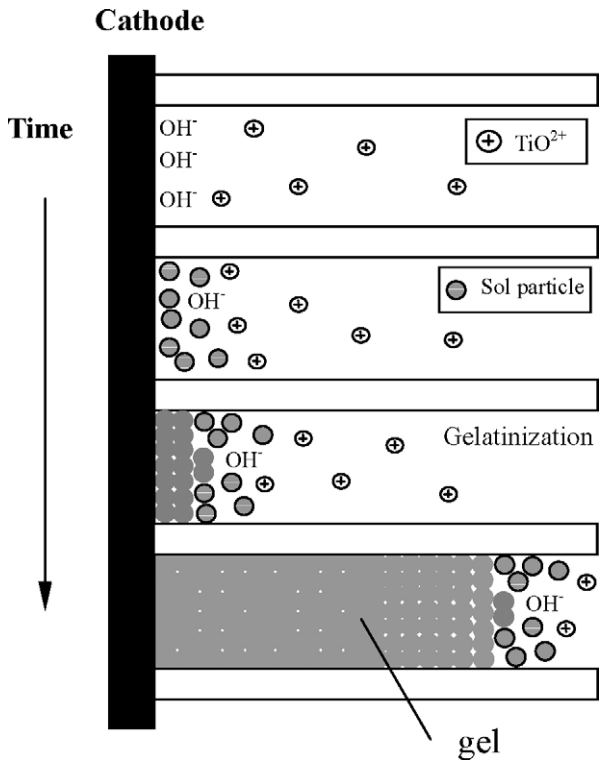

Fig. 4. Scheme for the electrochemically induced sol–gel process. Reprinted with permission from [90]. ©American Chemical Society (2002).

to the cathode. For the electrophoretic growth, the nanoclusters will migrate and deposit at the bottom of the pore under an applied electric field. Simultaneously, the counter ions move in the opposite direction. As time increases, the densely packed sol particles fill more of the pore, until the pore is completely filled. Finally, desired crystal structure of the oxide nanorods was achieved by a heat treatment (500–700 °C for 15–30 min) for crystallization and densification.

A number of single metal oxides (TiO_2, ZnO, SiO_2) and complex oxides ($BaTiO_3$, $Sr_2Nb_2O_7$, and $Pb(Zr_{0.52}Ti_{0.48})O_3$) [83–88] have been prepared by this sol–gel electrophoretic deposition. In addition, Cao and co-workers demonstrated that this method could be exploited to generate nanorods of hierarchically structured mesoporous silica [85]. Interestingly, Wan and co-workers have demonstrated that fullerene nanowire arrays were prepared in a cluster suspension of C_{60} by electrophoretic deposition [89].

2.1.6. Electrochemically induced sol–gel synthesis

Although the sol–gel electrophoresis deposition is widely applicable for the template growth of various oxide and complex oxide nanorods, this approach is still limited by the pore sizes of the templates used. Synthesis of nanorodes with diameter less than 50 nm is unsuccessful, due to the difficulty of diffusion of nanoclusters in the small nanosized pores [83–89]. In addition, serious shrinkage and cracking are also observed in these nanorods by electrophoresis deposition [82–84]. HRTEM images and electron diffraction patterns reveal that theses nanorods are polycrystalline, with small grains that are ~5 nm in size [85].

Xu and co-workers reported an electrochemically induced sol–gel method to prepare TiO_2 single-crystalline nanowire arrays (Fig. 4) [90]. At first, the hydroxyl ion is generated due to the cathodic reduction, and then the generation of OH^- ions increases the local pH at the electrode surface resulting in titanium oxyhydroxide gel formation in the pores of the template. Finally, subsequent heat treatment and the removal of the AAO template

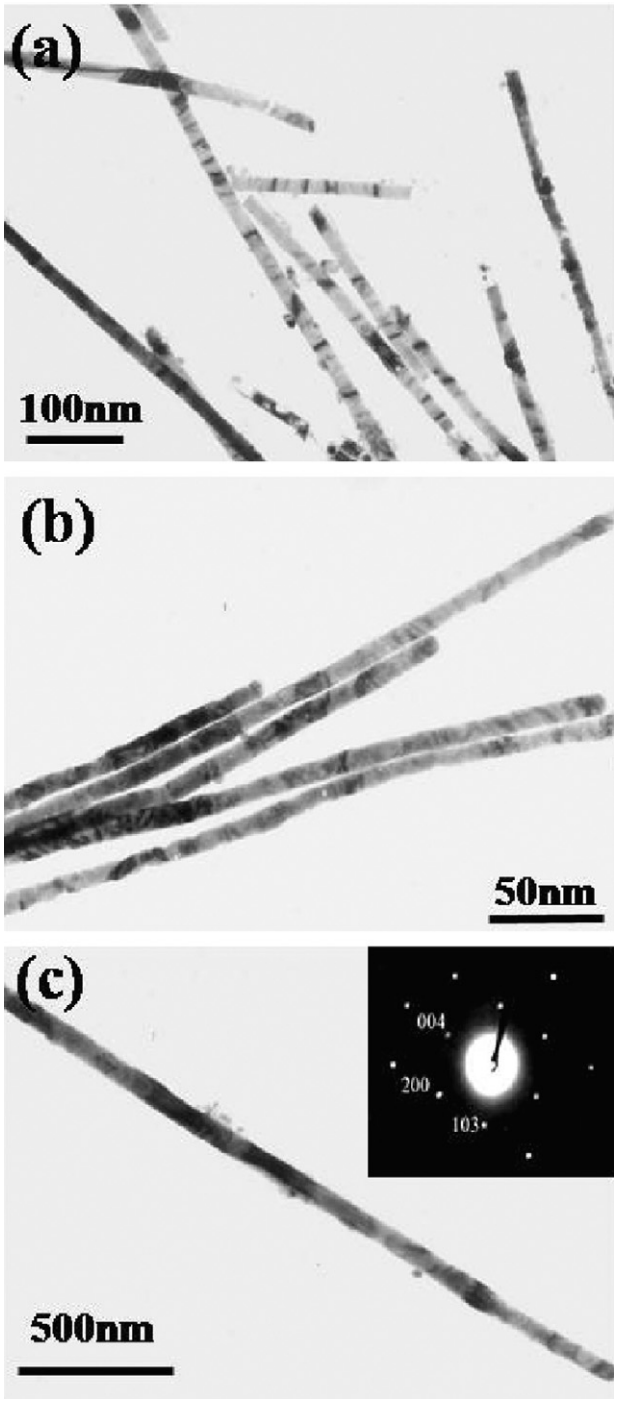

Fig. 5. TEM images of TiO_2 NWs grown in AAO membranes with pore diameters of (a) 22, (b) 12, and (c) 50 nm by an electrochemically sol–gel deposition process. The inset in (c) gives the corresponding selected area diffraction pattern. Adopted from [90]. ©American Chemical Society (2002).

results in the formation of TiO_2 single-crystalline nanowire arrays. During this electrochemically induced sol–gel process, both the formation of sol particles and the gelation process take place in the AAO pores.

This method offers several advantages for the formation of nanowires and nanotubes. Firstly, the sol–gel preparation of nanowires within the templates that have very small pores (less than 20 nm or even small) would be readily achievable by using this technique (Fig. 5). Secondly, the length of the nanowires can be controlled well by varying the deposition time and potential of the working electrode. Thirdly, less shrinkage and cracking will happen during the heat treatment of nanowires. The transport of ions through the voids of packed sol particles and the tiny pores in the titanium oxyhydroxide gel network courses the expansion of gel in the AAO pores and aging of the gel that has already formed. The AAO template with pores of nanoscaled size can restrict the diffusion of OH^- in solution, so it is easy to construct high local pH and long diffusion depth in the AAO pores, resulting a higher packing density gel.

Furthermore, Xu and co-workers demonstrated that the electrochemically induced sol–gel deposition is a general method for the growth of 1D nanostructures of a variety of inorganic oxides (single or complex) materials in small-pore templates. For example, one-dimensional silica nanostructures, such as nanotube, "bamboo-like" structures and nanowires have also been synthesized by such an electrochemically induced sol–gel deposition [91]. In addition, Zhang and co-workers synthesized TiO_2 nanowire arrays in AAO membranes by anodic oxidative hydrolysis of $TiCl_3$ [92,93]. Cao and co-workers reported that single-crystal V_2O_5 nanowire arrays with a growth direction of [0 1 0] were grown by anodic electrodeposition from $VOSO_4$ aqueous solution [73].

2.1.7. Others

Hybrid electrochemical/chemical strategies have been used to grow semiconducting NWs. They commonly involve two steps: the growth of metal NWs first by DCED and then the transferring these metal nanowires to metal compound NWs by chemical reactions. Various metal oxide NWs, including ZnO [94], SnO_2 [95], and CuO [106], have been fabricated by an electrodeposition and thermal oxidization methods. In these cases, the composition of the metal oxide nanowires is decided by the annealing temperature and the oxidation time [95]. Moreover, CdS nanowires have been fabricated by sulfurization of metal nanowires in S vapor at 300 °C for 30 h [96]. Another example is the conversion of metal Ag to Ag_2Se in Se vapor [65].

Furthermore, surfactant mesophases, including liquid crystals, vesicles, micelles, microemulsions and so on, have proven to be useful and versatile "soft" templates, in contrast to porous "hard" templates such as AAO membranes, track-etched polycarbonate and mica, zeolite/mesoporous silica, diblock copolymer matrix, etc. Unlike hard template-assisted electrochemical synthesis of NWs wherein the electrochemical synthesis of the desired materials is completely confined in the nanochannel of the template, selectively adsorption of organic surfactant molecules on a growing surface has a significant impact on the NW growth direction. Meanwhile, the surfactant mesophases may transform due to the phase separation during electrochemical synthesis or under the effect of an electric field. Huang et al. [107] reported that Cu_2O NWs with diameter of 25–100 nm were electrodeposited from anionic surfactant sodium bis(2-ethylhexyl) sulfosuccinate hexagonal liquid crystalline phase. The NWs can be grown to up to tens of micrometers in length by simply changing the electrodeposition time. Meanwhile, they have synthesized conductive polyaniline NWs in emeraldine form by potentiodynamic electropolymerization and single-crystalline silver NWs from the same reverse hexagonal liquid crystalline phase [108,109].

2.2. Direct electrochemical growth using capping reagents

Similar to colloidal synthesis, the capping reagents also play an important role in the shape evolution of the electrodeposited crystals [110–113]. Due to anisotropy in adsorption stability, these additives adsorb onto a certain crystallographic plane more strongly than others, which lowers the surface energy of the bound plane and hinders the growth of crystals on some crystal planes.

Consequently, the stability of crystallographic planes is destroyed, resulting in a change in the final morphology [114].

In many electrodeposition cases in aqueous baths, $[Zn(OH)_4]^{2-}$ ions, the growing unit, preferentially adsorbed on the positive polar face of the (0 0 0 1) surface results in faster growth along the ⟨0 0 0 1⟩ direction and in the formation of the rod-like deposits. Several studies have reported that oriented ZnO nano/microrod films have been epitaxially electrodeposited on a variety of single-crystalline substrates such as Au, Si, GaN, and InP [115,116].

However, the habited rod-like ZnO crystals are commonly smaller in the ratio of length-to-diameter. With preferential adsorption of capping reagents on the lateral $\{0\,1\,\bar{1}\,0\}$ surfaces group, the growth along the side direction may be largely limited and the relative growth rate along the ⟨0 0 0 1⟩ direction is enhanced. Xu et al. demonstrated that with additive of EDA molecules, homogeneous taper-like nanostructures over several cm^2 are routinely obtained on ITO substrates [1 1 0] (Fig. 6). Furthermore, as blocking simultaneously both EDA and Cl^- on the lateral $\{0\,1\,\bar{1}\,0\}$ surfaces group and the (0 0 0 1) face, the contraction rate of the (0 0 0 1) face decreases, and densely and oriented hexagonal ZnO nanorod films were formed (Fig. 7). In addition, a significant variation of the diameter and length of the electrodeposited ZnO nanorods was observed by changing only the nature of the anions in the solution [117].

Moreover, Yang et al. [118,119] reported an electrochemical route for the fabrication of ordered ultrathin ZnO nanorod/nanobelt arrays on a Zn electrode substrate in the presence of amine. In this case, ultrathin ZnO nanorod/nanobelt arrays were cathodically deposited in a two-electrode Zn–Zn cell from a mixed solvent bath containing H_2O, isopropanol, diethylamine and H_2O_2. Both ZnO nanobelts and ZnO nanorods as thin as 8 nm in ordered arrays were obtained.

3. Electrochemical synthetic strategies for oriented nanotube arrays

3.1. Multi-step template replication methods

Inorganic tubular structures have aroused intense interest because of their exceptional physical properties and potential applications in catalysis, sensor, solar cells and building blocks for nanodevices as well [120–122]. In particular, much effort has been devoted to the controllable synthesis of nanotubes by ED with the assistance of the template, such as AAO. An example for template-assisted electrochemical growth of metal oxide nanotubes is reported by Li et al. [123], in which polycrystalline ZnO nanotubes were directly electrodeposited in an AAO membrane from 0.01 M $Zn(NO_3)_2$ solutions at potentials of 1.5–1.8 V. However, direct electrodeposition in the template often leads to producing nanowires rather than nanotubes arrays. To avoid this problem, surface modification of the template's walls with organic molecular or inorganic nanoparticles is adopted to induce the preferentially electrodeposition on the pore walls to produce the nanotubes [124,125].

Recently, Xu and co-workers [126] developed a general process to fabricate uniform inorganic nanotube arrays through a multi-step template replication and electrodeposition approach (Fig. 8). This approach involves the deposition of carbon nanotubes (CNTs) on the interior walls of the AAO templates, electrodeposition of Ni into the pores of the CNTs/AAO membranes to form a coaxial Ni/CNT/AAO nanocable structure, burning off the CNTs in the template membranes to yield a highly ordered annular nanochannel membrane, loading the desired inorganic materials into these annular nanochannels, and finally chemical dissolution of the NiO core and the AAO membrane to expose the produced nanotubes.

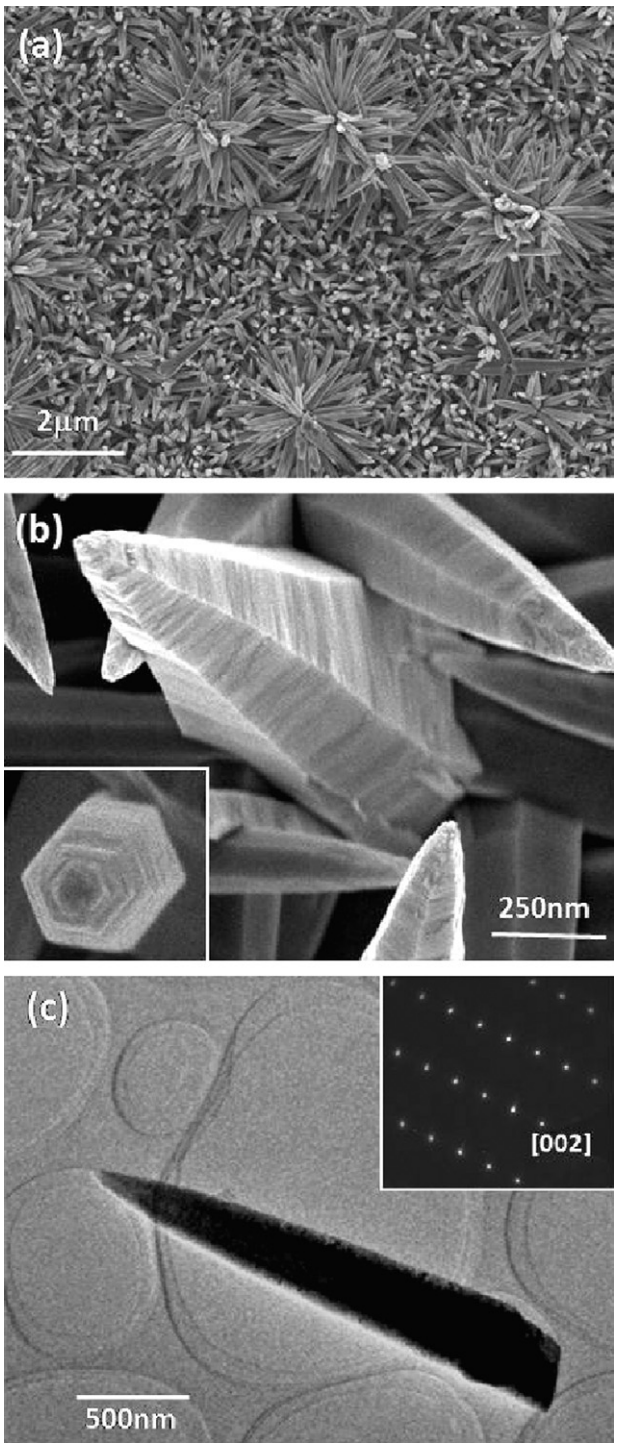

Fig. 6. (a and b) SEM and (c) TEM images of the taper-like ZnO nanostructures by electrodeposition from solutions containing 0.05 M $Zn(NO_3)_2$ and 0.013 M EDA. The inset in part (c) is an electron diffraction pattern corresponding to the [0 0 1] zone axis of a ZnO single nanotaper. Adopted from [110]. ©American Chemical Society (2005).

A variety of template synthesis strategies could be employed to control the nanotube growth in these annular nanochannels. For example, highly ordered nanotube arrays of metals (Pt, Au, Bi, In, Cu) and semiconductors (CdS, CdSe, CdTe, etc.) were synthesized by dc electrodeposition into the annular nanochannels [126]; uniform Si nanotube arrays were prepared by vapor deposition of Si into the annular nanochannels using pyrolytic decomposition of SiH_4 at 650 °C in argon atmosphere [127]. As seen in Fig. 9,

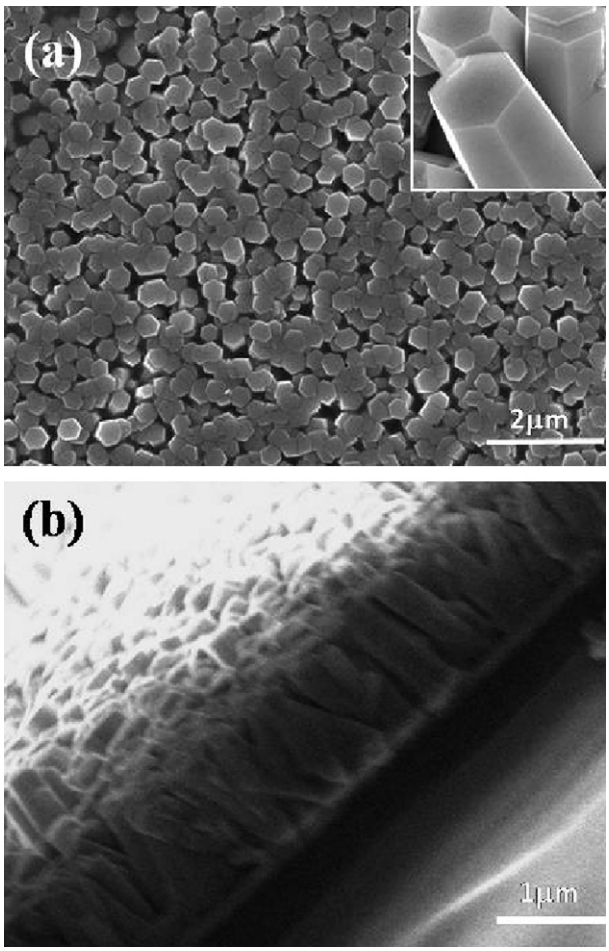

Fig. 7. SEM images of the ZnO nanostructures by electrodeposition from solutions containing 0.05 M $Zn(NO_3)_2$ and 0.06 M KCl and 0.01 M EDA: (a) top view and (b) side view. Reprinted with permission from [110]. ©American Chemical Society (2005).

these Si nanotubes are uniform both in their morphologies and wall thickness. Since the wall thickness of the CNTs increases with the pyrolytic decomposition time, the wall thickness of the nanotubes can be adjusted by simply controlling the deposition time of the CNTs.

3.2. Two-step synthetic strategy

Several studies also have been reported in the preparation of single-crystalline nanotubes by a two-step synthetic strategy [128–131]. In general, this strategy involves the electrodeposition of oriented ZnO nanorods and subsequently selective dissolution of ZnO along the *c*-axis to form tubular structure. The inner/outer wall surfaces of the obtained ZnO nanotubes are quite smooth and the wall thickness is uniform (Fig. 10a–d). Furthermore, the etching process starts from the center of the top surface and then slowly to the interior of the rod, as proved by the SEM images (Fig. 10e–g). Meanwhile, the wall thickness of the nanotubes decreases with the dissolution time [128]. In addition, with the aid of the external voltage, ZnO nanotubes could also be achieved at the particular position of the substrate [131].

Xu et al. proposed that the formation process of the nanotubes can be proposed as a coordination-assisted selective dissolution mechanism [128]. Treatment of ZnO rods in EDA served two aims: dissolution of the ZnO rods and selective coordination on specific crystal faces. In aqueous EDA solution, hydroxyl ions are formed by the hydrolysis of EDA and are further reacted with ZnO to form soluble hydroxyl complex such as $[Zn(OH)_4]^{2-}$.

$$(CH_2NH_2)_2 + 2H_2O \rightarrow (CH_2NH_3)^{2+} + 2OH^- \quad (4)$$

$$ZnO + 2OH^- + H_2O \rightarrow [Zn(OH)_4]^{2-} \quad (5)$$

On the other hand, EDA is a type of molecule with strong coordination ability to zinc. The preferential adsorption of EDA molecule occurs on the lateral $\{0\,1\,\bar{1}\,0\}$ surfaces rather than on the (0 0 0 1) ones. Meanwhile, OH^- anions preferentially adsorb on the (0 0 0 1) surface of the ZnO rod because of the electrostatic adherence. The adsorbed EDA molecule may provide electrons to Zn atoms, change the distribution of the charges between Zn and O atoms, and enhance the Zn–O bond. As a result, the ZnO dissolution rate at the edge of the (0 0 0 1) surface would be much slower than in the center. The selective dissolution of ZnO along the *c*-axis causes the formation of the tubular structure.

Moreover, Tang et al. [132] reported a direct electrodeposition method for the fabrication of single-crystalline ZnO nanotube arrays on F-doped SnO_2 substrates. Control experiments demonstrated the dramatic influence of the surface conditions of the substrate material and the experimental conditions on the morphology of the product layer. For example, single-crystalline ZnO nanotube arrays were obtained at potentials of −0.70 V vs. SCE, while ZnO nanorod arrays were prepared at potentials higher than −0.8 V. The formation of the nanotube array was attributed to the epitaxial growth along the nanowires forming at the early stage.

3.3. Anodization methods

Since the first report on formation of TiO_2 nanotube via anodization in an aqueous electrolyte with HF by Grimes and co-workers in 2001 [133], TiO_2 nanotube arrays (TNT) are of great interest because they show some advantages in potential applications such as photocatalysis, sensing, photoelectrolysis, and photovoltaics [134]. In the next decade, many groups tried to optimize the conditions of the anodization to fabricate TiO_2 nanotube arrays with much better structures. Using non-aqueous electrolyte, such as glycol, diethylene glycol, glycerol, or DMSO, provided more precise control of the nanotube morphology [135–139]. The TiO_2 nanotube arrays

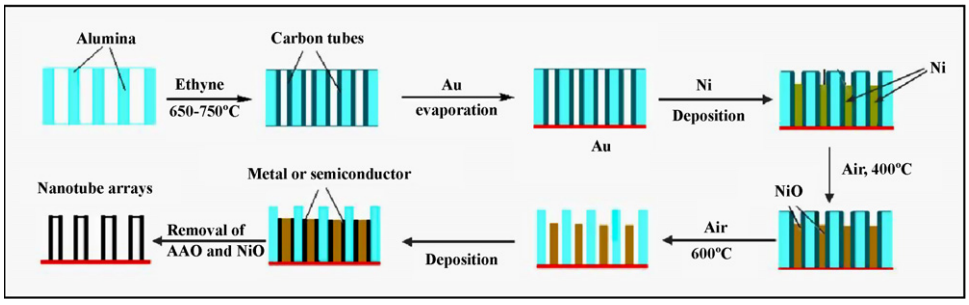

Fig. 8. Flow chart of the multi-step template replication process for preparation of uniform nanotube arrays. Adopted from [126]. ©John-Wiley (2004).

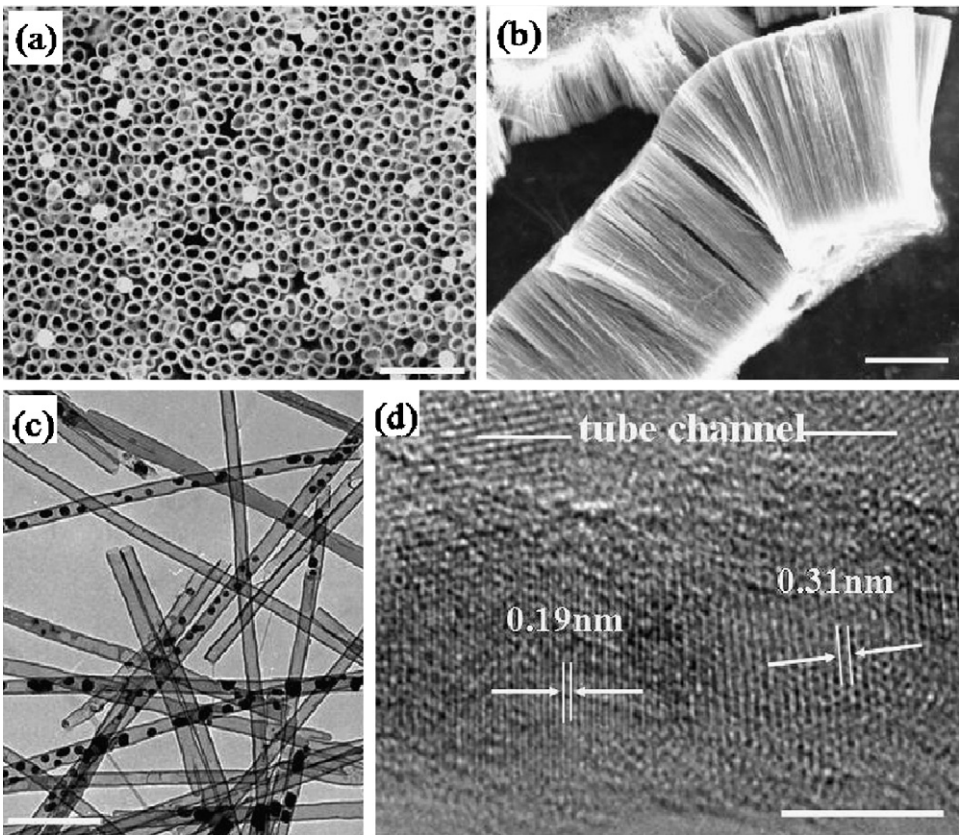

Fig. 9. (a and b) SEM and (c and d) TEM images of the SiNTs arrays after partial removal of the AAO pore wall and the nickel oxide cores: (a) top view and (b) side views. Scale bar: (a) 400 nm, (b) 10 μm, (c) 250 nm, and (d) 5 nm. Adopted from [127]. ©American Institute of Physics (2005).

formed with high regularity and homogenity in highly viscous glycerol electrolytes owing to the suppression of local concentration fluctuations and pH bursts during anodization [135]. Moreover, the water content in the electrolyte can affect the speed of chemical dissolution of TiO_2, which determines the length of the nanotube arrays [136]. In addition to the factors above, applied potential, concentration of fluoride ions and time also have impact on the morphologies of the nanotube arrays [138]. Under optimized conditions, high aspect ratio nanotube arrays of about 250 μm have been successfully achieved. Furthermore, double-walled TiO_2 nanotubes can be prepared in fluoride-containing electrolytes through adjusting the anodization condition and heat treatment process [140]. TiO_2 nanobamboo nanotubes rather than uniform nanotubes also can be attained using alternating-voltage anodization method [141]. Chemical transformation of the synthesized TiO_2 nanotube arrays also provides another way to produce nanotube arrays of other materials [142,143].

After anodizing Ti to get the nanotubes, it is preferred to remove the blocking layer between nanotube arrays and Ti substrate, because the blocking layer will constrict the transport of electrons. For instance, Schmuki's group developed a method through dissolution of the Ti substrate in water-free CH_3OH/Br_2 solution [144]. Other ways to detach the TNT arrays from the Ti substrate can be achieved through ultrasonic cleaning [145], solvent-evaporation methods [146] or immersing the arrays in aqueous HCl [147]. Recently, Chen et al. reported than TNT arrays with different length could be produced through ultrasonication in a mix solution of ethanol and water [148]. Although some progress has been made on the preparation of the free-standing TNT arrays, it is still difficult to fabricate large-scale, noncurling, and free-standing crystallized TNT arrays. Because of the amorphous property of the amorphous after anodization, direct crystallization at high temperature often lead to crashing or curling of the arrays. Trying to avoid this problem, Xu's group has developed a newly two-step anodization method [149], as illustrate in Fig. 11. First, Ti sheet was anodized in the fluoride-containing electrolytes to produce amorphous TNT arrays. Second, the former TNT arrays were annealed at high temperature to crystallize them. After taking the second anodization of the film, the free-standing crystallized TNT arrays were successfully obtained through dissolution of the second amorphous TiO_2 by H_2O_2. As shown in Fig. 12, free-standing crystallized TNT arrays with different lengths can be successfully prepared by adjusting the anodization voltages and time.

4. Electrochemical synthetic strategies for complex hierarchical nanostructured films

Hierarchical assembly of one-dimensional nanostructures (nanotubes, nanowires, or nanobelts) is essential for the success of bottom-up approaches toward future nanodevices. Much effort has been devoted to assemble nanorod/nanowire building blocks into two- and three-dimensional ordered superstructures or complex functional architectures. For instance, special architectures of nanorods, such as multipods, nanocombs, nanowindmills, nanowire and nanoribbon netstudies, penni-form structures, have recently been reported [150–159]. Moreover, complex nanostructures with nanotree morphologies induced by twist dislocation have been successfully prepared [160,161]. Although improvements have been widely achieved for single complex nanostructure, the assembly of them into a hierarchical film is still elusive.

Xu et al. presented a two-step electrochemical deposition process to produce various hierarchical ZnO nanostructures films such as 2-fold nanorod arrays on nanosheets, 6-fold nanorods

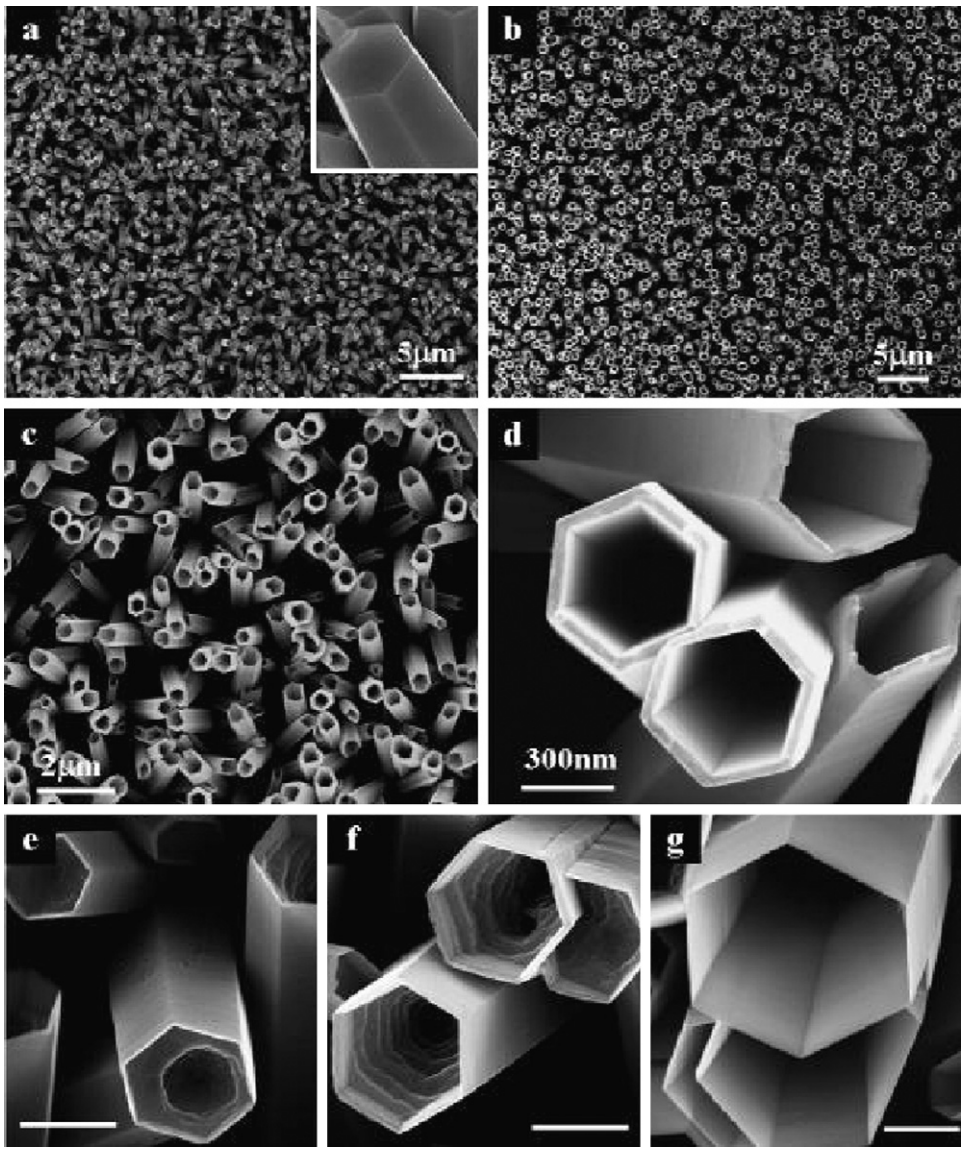

Fig. 10. SEM images of the electrodeposited ZnO nanorods (a) and the ZnO nanotubes by selective dissolution of the rods in 0.1 M EDA aqueous solution at 70 °C under a bias of −0.20 V vs. SCE for different reaction times: (b–d) 10 h, (e) 2 h, (f) 5 h, (g) 15 h. The scale bars: (e) 500 nm, (f) 500 nm, (g) 200 nm. Reprinted with permission from [128]. ©American Chemical Society (2007).

on nanorods, and 6-fold nanoneedles on nanoneedles [162]. This approach involves the electrodeposition of ZnO crystals with different controllable morphologies, and then the electrochemically epitaxial growth of oriented nanorods on the surfaces of the ZnO nanostructures obtained by the first electrodeposition. Fig. 13a presents a typical SEM image of hexagonal ZnO nanosheets on ITO substrates as obtained by electrodeposition from 0.05 M $Zn(NO_3)_2$ containing 0.06 M KCl. After 1.5 h of secondary electrodeposition in 0.05 M $[Zn(NH_3)_4]^{2+}$ solution, highly oriented ZnO nanorod arrays were grown on the primary nanosheets (Fig. 13b–d). A detailed time-dependent morphology evolution study indicated that the nanorods grew on the surfaces of the primary ZnO nanosheets (Fig. 14a–d). Moreover, the dense and oriented nanorods on hexagonal ZnO sheets could change to a beltlike (Fig. 14e) or hexagonal fence (Fig. 14f) structure composed of closely packed nanorods through prolonging the deposition time or slightly decreased the pH of the solution. Furthermore, 6-fold hierarchical structures of nanorods on nanorods, and 6-fold nanoneedles on nanoneedles were also synthesized by the same electrochemical strategy.

As we know, when the surface energy of the substrate is much smaller than that of the deposits, the growth of isolated 3D islands is more favored. The formation of isolated nanostructures of ZnO on the ITO substrates in the first-step electrodeposition indicated that potential barrier of the crystal nucleus formation and subsequent growing into a perfect crystal of ZnO on ITO-coated glass is much higher than that on ZnO itself. Therefore, during the secondary electrodeposition, the ZnO deposits would grow preferentially on the surface of the primary ZnO crystals rather than the ITO substrate, leading to the growth of the hierarchical nanostructures. In addition, the growth of the oriented ZnO nanorods on the ZnO nanocrystals may be attributed to a balance between $[Zn(NH_3)_4]^{2+}$ and the growth unit of $[Zn(OH)_4]^{2-}$. In the beginning of the secondary electrodeposition, large amounts of $Zn(NH_3)_4{}^{2+}$ ions in the solution can easily turn into the growth units of $[Zn(OH)_4]^{2-}$, which lead to the crystal nucleus formation on the surfaces of the ZnO nanocrystals and subsequent growing into a perfect crystal of ZnO along [0 0 0 1].

In addition to above method, Cao et al. reported a seed-layer assisted electrochemical deposition route for preparation

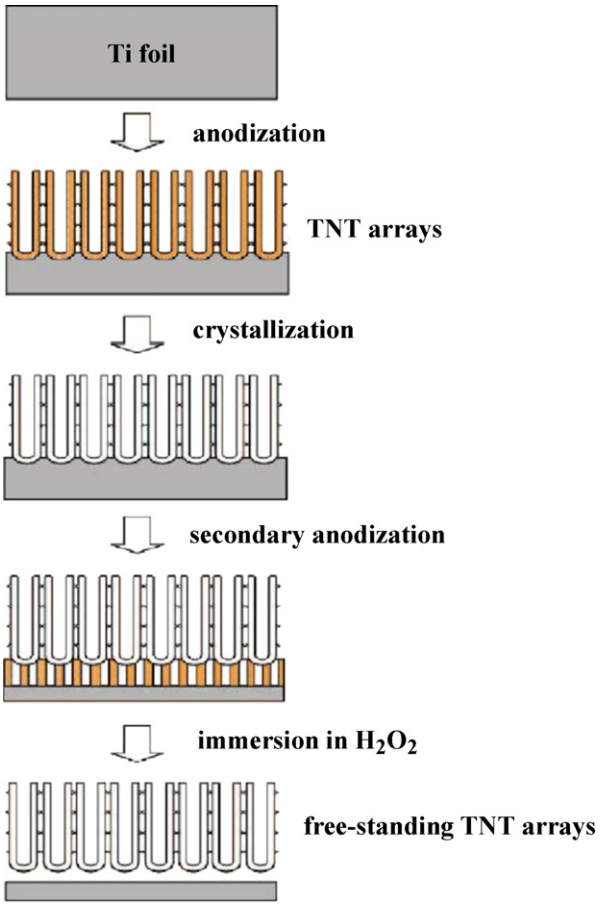

Fig. 11. Schematic illustration of the procedure for preparing free-standing crystallized TNT arrays. Reprinted with permission from [149]. ©American Chemical Society (2009).

of different ZnO nanostructures [163]. Hierarchical ZnO nanostructured arrays of nanowires, microcalabashes and nanoplates are fabricated at the deposition current of 1.0, 1.25 and 1.5 mA, respectively. Li et al. [164] demonstrated that the ZnO dendritic nanostructures were prepared on Cu substrates by electrodeposition in aqueous $ZnCl_2$ solutions and adding citric acid as a shape-control agent.

5. Structures, properties and applications

5.1. Crystal structure

Crystal structure of the semiconductor nanowires, e.g. single crystal, polycrystalline or amorphous, plays a key role in nanodevices and other applications. The crystal structure of nanowires greatly depends on the experimental conditions, the electrochemical methods, etc. For instance, the CdSe NWs prepared by DCED from a non-aqueous bath mostly crystallized as a uniform orientation, i.e. [0 0 1], as well as highly ordered arrangement in morphology [56]. The XRD data also indicated that the *c*-axis of hexagonal crystals is preferentially aligned along the direction normal to the substrate rather than oriented randomly. The similar crystalline orientations have also observed on other semiconductor NWs prepared by DCED from non-aqueous baths [57,58]. However, in aqueous baths, the deposited NWs are randomly oriented [63,65].

To enhance the crystallinity of the nanowires by electrodeposition, thermally annealing at high temperature is an effective method. For example, the unit cell of the as-deposited CdS nanowire was found to be compressed with respect to that of polycrystalline. The interplane spacing, d_{002}, of as-deposited samples shows a nonmonotonic dependence on diameter. Annealing at 500 °C for 1 h successfully relieved this distortion, leaving a slight residual increase in d_{002} with nanowire diameter, and caused the grain sizes of the CdS deposit to increase, except for nanowires with small diameters [31]. Moreover, the degree of the crystalline orientation also increased by annealing. After annealing and a slow cooling, (0 0 2) and (0 0 4) diffraction peaks of β-Ag_2Se appeared with strong intensities. Meanwhile, the intensities of other primary diffraction peaks e.g. (1 1 2) and (1 2 1) are almost suppressed in comparison with the XRD pattern before annealing. For electrochemical sol–gel synthesis, the annealing process is very important to obtain condense and highly crystalline nanowires [83–91].

The deposition of the nanowires controlled by electrochemical reaction usually results in a polycrystalline structure. These problems can be avoided if the deposition is controlled by a chemical reaction rather than by the electrode kinetics [82]. Another example is single-crystal anatase TiO_2 nanowires by electrochemically induced sol–gel strategy [90]. In contrast to the single-crystalline TiO_2 nanowires by electrochemically induced sol–gel deposition, the TiO_2 nanowires by sol–gel electrophoretic deposition are polycrystalline with grains that are ~5 nm in sizes, characterized by HRTEM and electron diffraction patterns [85].

5.2. Free-standing 1D nanostructure arrays

In the template-assisted electrochemical synthesis approaches, the nanowires are assembled with morphology complementary to that of the template. Because the nanopores with monodisperse diameters are uniformly and hexagonally spaced perpendicular through the AAO membrane, the nanowires embedded in the template form highly ordered and vertically aligned nanowire arrays. However, after the template was removed, the embedded nanowire arrays would collapse into a tangled mass. Although some nanorodor nanotube arrays with short aspect ratios have been successfully prepared on the substrate after removing the template [165,166], the collapse of the nanowire arrays is a common phenomenon. Generally, the nanowire arrays were congregated into bundles by natural drying after dissolution of the template, completely detached from the substrate or broken in the length direction of the wires. It is reasonable that the surface tension force exerted on the nanowires during the evaporation of the liquid is the reason for the collapse during natural drying process.

To avoid the liquid–gas interface and thus eliminate a surface tension force during the liquid evaporation, supercritical drying is used to obtain non-collapsing and vertically aligned nanowire arrays [167]. In the supercritical drying process, we successfully avoided liquid–gas interface in all the steps including AAO dissolving, ethanol-exchanging, and the phase transformation of CO_2 from liquid to supercritical then to gas phase. Therefore, the surface tension force would be eliminated. As a result, the nanowires would keep their vertically aligned state after the removal of the template just as they were embedded in it. Fig. 15a displays the SEM images of the samples by the supercritical CO_2 drying process. Large-area, non-collapsed and vertically aligned nanowire arrays are formed. These nanowire arrays do not aggregate and the nanowires keep their hexagonally packed pattern after the removal of the template as if they were still embedded in template. The side view image (Fig. 15b) indicates that the AAO has been completely dissolved and the nanowires are vertically aligned on the Au film substrate, which ensures a conductive contact between the nanowires and the substrate.

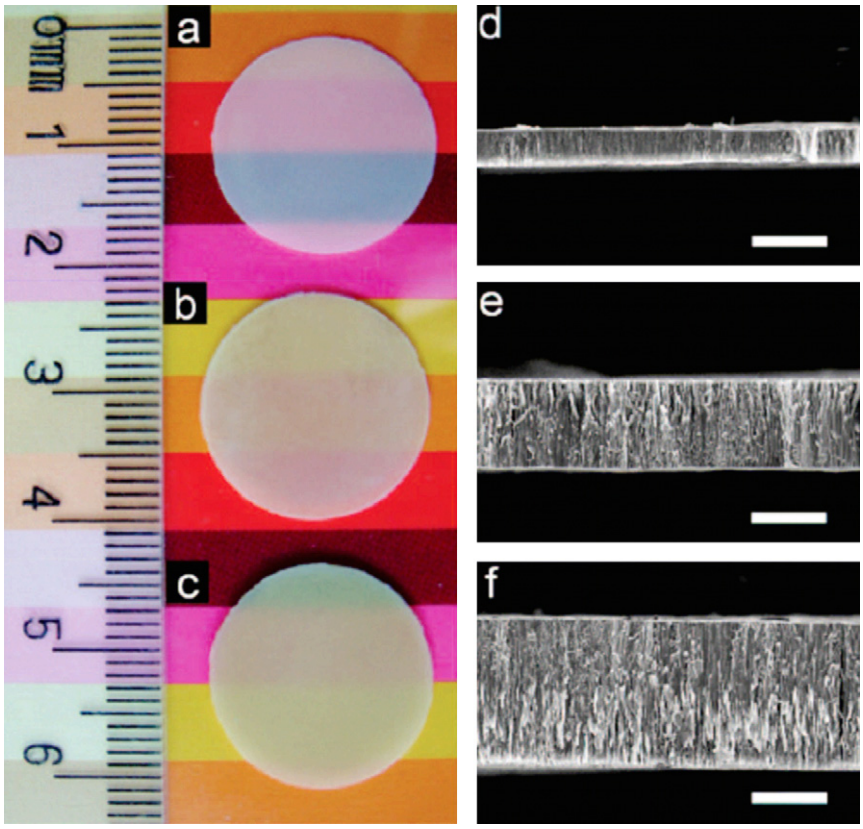

Fig. 12. Optical images of translucent free-standing crystallized TNT membranes prepared in ethylene glycol at 30 V for 72 h (a) and at 50 V for 24 h (b) and 48 h (c). The right column is the corresponding SEM images of the cross-section of the membranes with different thicknesses of 9 μm (d), 25 μm (e), and 42 μm (f). The scale bar is 20 μm. Reprinted with permission from [149]. ©American Chemical Society (2009).

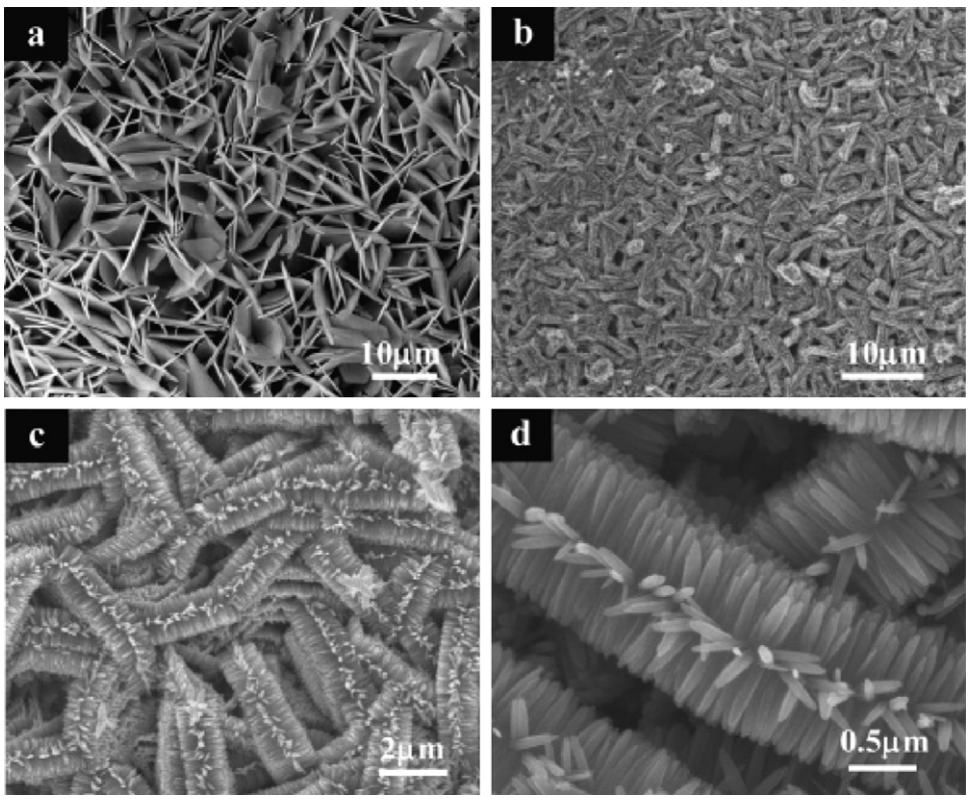

Fig. 13. SEM images of (a) primary ZnO nanosheets and (b–d) hierarchical ZnO nanorods on hexagonal nanosheets on ITO substrates. Reprinted with permission from [162]. ©American Chemical Society (2007).

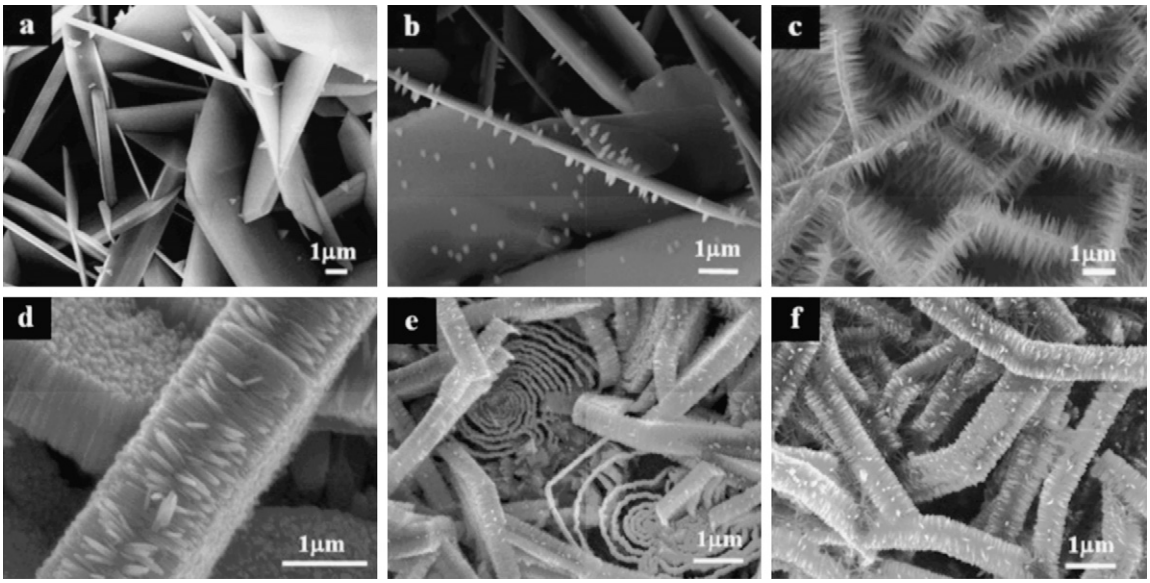

Fig. 14. SEM images of hierarchical ZnO nanostructures electrodeposited at a potential of −1.10 V in 0.05 M $[Zn(NH_3)_4]^{2+}$ solution for different deposition times: (a) 10 min, (b) 20 min, (c) 40 min, (d) 1.5 h, (e) 2.5 h, (f) 3.5 h. Reprinted with permission from [162]. ©American Chemical Society (2007).

5.3. Energy-band engineering through composition modulation

One of the most important parameters characterizing semiconductor nanowires is their band-gap energy, which determines many of their gross electronic and optical properties. The most straightforward to determine the band-gap energy is the measurement of the low-energy optical absorption band-edge. Aside from varying the nature of the semiconductor nanowire itself, it is also possible to control the band-gap energy of a given semiconductor by restricting the dimensions to values below that of the excitonic Bohr diameter [168]. Peng et al. have measured the optical absorption of the DCED fabricated Bi_2S_3 nanowire arrays embedded in the AAO membranes [61]. They considered that the excitation band is not likely to be present and the absorption is due to a band-to-band transition. The band gap of Bi_2S_3 nanowires is deduced to have a value of about 1.56 eV, which is larger than one of the bulk Bi_2S_3 (1.3 eV).

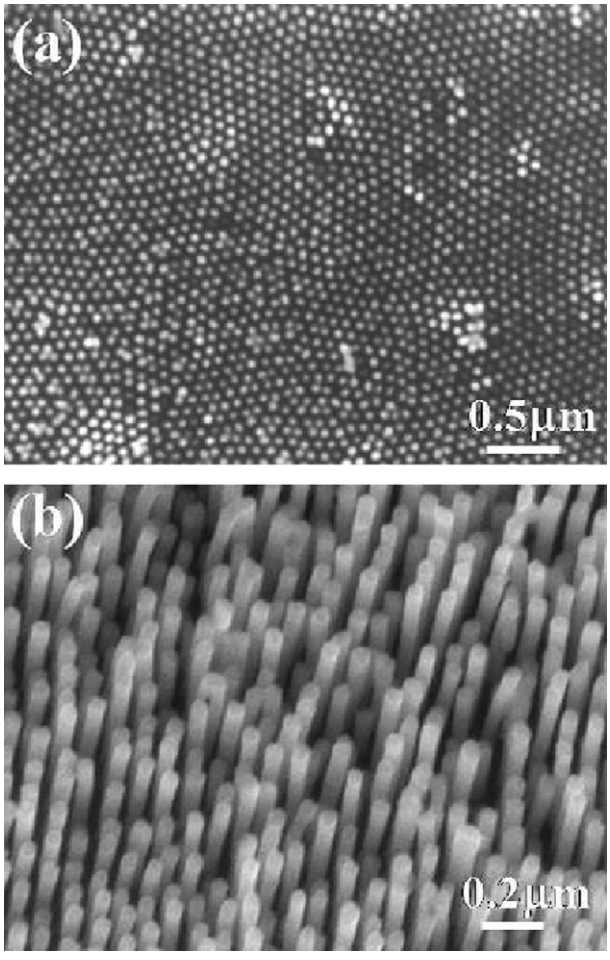

Fig. 15. SEM images of the supercritical drying samples: (a) low magnification, (b) higher magnification. Adopted from [167]. ©American Chemical Society (2004).

Another way to engineer the energy-band of the NWs is based on composition modulation, which is widely used in 2D II–VI and III–V based semiconductors film configuration [97]. Similar to the ideas in 2D counterpart, designed energy-band engineering of nanowires is expected to yield nanoscale devices with interesting properties and functions. Xu and co-workers [79] present a class of alloyed II–VI semiconductor-ternary $CdS_{1-x}Se_x$ nanowires by DCED. Energy dispersive X-ray (EDX) and XRD results indicated that no excess amount of Cd was found. HRTEM image shows these alloyed $CdS_{1-x}Se_x$ nanowires have a single-crystalline structure. Optical measurements indicate that band gaps of these well-structured nanowires are continuously tuned from 1.7 eV (CdSe) to 2.4 eV (CdS). The corresponding fluorescent emission of the $CdS_{1-x}Se_x$ nanowires also can be continuously tuned from 715 nm (CdSe) to 511 nm (CdS) when the Se concentration gradually decreased, as shown in Fig. 16. The observed typical full-width at half-maximum (FWHM) of the band-edge fluorescence for these nanowires is 30 to 40 nm, which is comparable to those of the widely used II–VI quantum dots [169].

5.4. Photoluminescence (PL) properties

Many unique and fascinating properties have been proposed and demonstrated for SNWs, such as oriented transport of carriers, order-of-magnitude polarization anisotropy of photoluminescence and laser emission [4]. Luminescent emission from SNWs by electrochemical synthesis has been observed. For instance, a blue and a blue-green PL band were observed in ZnO [92,93] and In_2O_3

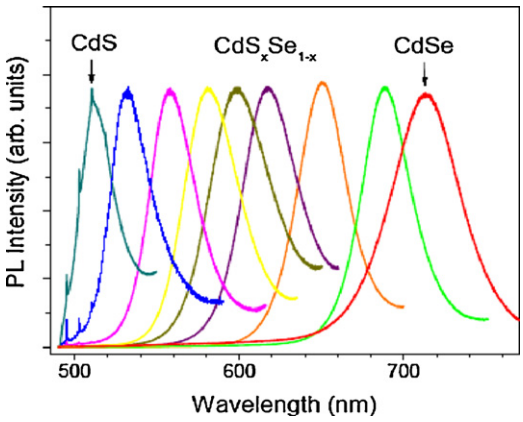

Fig. 16. The fluorescent emission spectra of a series of $CdS_{1-x}Se_x$ nanowires. All the samples were excited with a 488 nm Ar^+ laser at room temperature. Adopted from [79]. ©American Chemical Society (2005).

[95] nanowires, respectively. On the other hand, these aligned SNW arrays could be used for the nanowire lasers. Recently, room-temperature ultraviolet lasing in (0 0 0 1) oriented zinc oxide nanowire arrays grown on sapphire substrates has been demonstrated by Huang et al. [21]; these are expected to serve as miniaturized light sources for microanalysis, information storage, and optical computing. Due to their highly crystalline and well-oriented properties, SNW arrays by electrochemical synthesis, such as ZnO, CdS, CdSe, CdTe, etc., are good candidates for excitonic laser action.

5.5. Photovoltaics and photocatalysis

The SNW arrays could be used as a new class of electrodes for photovoltaics. One of the important applications of these nanowire electrodes could be the "Grätzel solar cell". Conventional cell is based on nanoporous and nanocrystalline TiO_2 on which a monolayer of a photosensitizer is absorbed. Replacing nanoparticles with nanowires would benefit for transporting the electron, which was one of the bottlenecks in the conventional Grätzel cell. With nanowire electrodes, electrons can be transported directly to the conducting substrate without going through the multiple steps of the tunneling process. This is expected to greatly decrease the probability of recombination across the large heterogeneous interface and improve the overall efficiency of the solar cell. In addition, semiconductor CdSe nanorods can be used to fabricate readily processed and efficient hybrid solar cells together with polymers [170]. As the aspect ratio of the nanorods increases from 1 to 10, the charge transport must improve substantially to yield an external quantum efficiency enhancement by a factor of approximately 3. Besides SNW arrays, TNT arrays are also an ideal option for dye-sensitized solar cell (DSSC). It has been experimentally proven that the NT-based DSSCs have significantly higher charge-collection efficiencies than their NP-based counterparts. Meanwhile the higher light-harvesting efficiencies owing to stronger internal light-scattering effects can also improve their performance [171]. The electron diffusion length of the TNT cells is of the order of hundreds micrometers [172]. Moreover, the short circuit-current of the cell can also be improved through $TiCl_4$ treatment to increase the specific dye loading [173]. In addition, Xu and coworkers also presented that a 25 μm-thick free-standing crystallized TNT arrays in DSSC showed an efficiency of 5.5%, indicating a roughly 100% enhanced conversion efficiency compared with that of the TNT array on a Ti substrate [149].

Furthermore, these nanowire arrays could be used as photocatalysts for light-induced redox processes. The photocatalytic reaction involves absorption of a UV photon by semiconductor (i.e., TiO_2) to produce an electron–hole pair and then trapping of the electron or hole by scavengers or surface defects. The valence band holes are powerful oxidants while the conduction band electrons are good reductants. For example, the generated holes have been used to oxidize organic molecules for environmental remediation applications. Lakshmi et al. have investigated the decomposition of salicylic acid over time on an array of immobilized TiO_2 fibres with exposure to sunlight [98,99]. Moreover, Schmuki's group reported that the TNT arrays can be more efficient photocatalysts than comparable nanoparticles [174]. Their photocatalytic activity can be further enhanced by noble metal deposition [175] or applying an external bias [176].

Grime's group examined the use of TNT arrays for the photocleavage of water into hydrogen and oxygen gas under ultraviolet irradiation [177]. The nanotube wall thickness is a key parameter influencing the magnitude of the photoanodic response and the overall efficiency of the reaction. Meanwhile, the length of the tubes also affected the overall conversion efficiency, which can be achieved at 6.8% and 12.25% for hundreds of nanometers [177] and 6 μm [178], respectively. The further study indicated that under visible light AM 1.5 illumination (100 mW/cm^2) the titania nanotube array photoanodes with a photoconversion efficiency of 0.6% can be achieved [179].

6. Conclusion

In this review, we have discussed several electrochemical synthesis strategies that have been demonstrated for the synthesis of 1D semiconductor nanostructures: electrodeposition of materials in porous membranes with 1D pore geometry; template-free methods that electrodeposition 1D structures by kinetically controlling the growth rates of various faces through the use of capping reagents; methods that achieve uniform nanotube arrays by multi-step template replication, two-step synthetic strategy or anodization methods; electrochemical synthetic strategies for complex hierarchical nanostructured films. Different from other cost-intensive methods such as laser ablation or thermal evaporation synthesis, the electrochemical method provides an alternative simple and viable way to prepare 1D semiconductor nanostructures, and can also afford precise process control due to its electrical nature. For example, the aspect ratios and the compositions of the nanostructures can be simply modulated by the electrochemical parameters including the voltage, the deposition time and the electrolyte composition. In general, the 1D semiconductor nanostructures by electrochemical deposition are highly crystalline and aligned on the conductive substrates. They could have very important applications in nanosensors, photocatalysis, solar conversion devices, and planar displayers.

Acknowledgements

This work was supported by the Major State Basic Research Development Program (Grant No. 2000077503) and the National Science Foundation of China.

References

[1] S. Iijima, Nature 354 (1991) 56.
[2] H.S. Nalwa, Handbook of Nanostructured Materials and Nanotechnology, Academic Press, 2000.
[3] K.J. Klabunde, Nanoscale Materials in Chemistry, John Wiley & Sons, Inc, 2001.
[4] Z.L. Wang, Nanowires and Nanobelts: Materials, Properties and Devices, Kluwer Press, 2003.
[5] R. Martel, T. Schmidt, H.R. Shea, T. Hertel, Ph. Avouris, Appl. Phys. Lett. 73 (1998) 2447.
[6] M. Bockrath, D.H. Cobden, J. Lu, A.G. Rinzler, R.E. Smalley, T. Balents, P.L. McEuen, Nature 397 (1999) 598.

[7] Z. Yao, H.W.C. Postma, L. Balents, C. Dekker, Nature 402 (1999) 273.
[8] R.S. Wagner, W.C. Ellis, Appl. Phys. Lett. 4 (1964) 89.
[9] A.M. Morales, C.M. Lieber, Science 279 (1998) 208.
[10] T.J. Trentler, K.M. Hickman, S.C. Goel, A.M. Viano, P.C. Gibbons, W.E. Buhro, Science 270 (1995) 1791.
[11] Y.T. Qian, Adv. Mater. 11 (1999) 1101.
[12] C.R. Martin, Acc. Chem. Res. 28 (1995) 61.
[13] C. Yang, Z. Zhong, C.M. Lieber, Science 310 (2005) 1304.
[14] L.J. Lauhon, M.S. Gudiksen, D. Wang, C.M. Lieber, Nature 420 (2002) 57.
[15] S.J. Tans, M.H. Devoret, H.J. Dai, A. Thess, R.E. Smalley, L.J. Geerligs, C. Dekker, Nature 386 (1997) 474.
[16] M. Bockrath, D.H. Cobden, P.L. McEuen, N.G. Chopra, A. Zettl, A. Thess, R.E. Smalley, Science 275 (1997) 1922.
[17] S.J. Tans, R.M. Verschueren, C. Dekker, Nature 393 (1998) 49.
[18] R. Martel, T. Schmidt, H.R. Shea, T. Hertel, P. Avouris, Appl. Phys. Lett. 73 (1998) 2447.
[19] J. Hu, M. Ouyang, P. Yang, C.M. Lieber, Nature 399 (1999) 48.
[20] Z. Yao, H.WC. Postma, L. Balents, C. Dekker, Nature 402 (1999) 273.
[21] M.H. Huang, S. Mao, H. Feick, H.Q. Yan, Y.Y. Wu, H. Kind, E. Weber, R. Russo, P.D. Yang, Science 292 (2001) 1897.
[22] Y.F. Huang, S. Chattopadhyay, Y.J. Jen, C.Y. Peng, T.A. Liu, Y.K. Hsu, C.L. Pan, H.C. Lo, C.H. Hsu, Y.H. Chang, Nat. Nanotechnol. 2 (2007) 770.
[23] N.R. Chiou, C. Lu, J. Guan, L.J. Lee, A.J. Epstein, Nat. Nanotechnol. 2 (2007) 354.
[24] F. Cheng, Z. Tao, J. Liang, J. Chen, Chem. Mater. 20 (2008) 667.
[25] X. Feng, K. Shankar, O.K. Varghese, M. Paulose, T.J. Latempa, C.A. Grimes, Nano Lett. 8 (2008) 3781.
[26] G.K. Mor, K. Shankar, M. Paulose, O.K. Varghese, C.A. Grimes, Nano Lett. 6 (2006) 215.
[27] C.R. Martin, Science 266 (1994) 1961.
[28] C.R. Martin, Acc. Chem. Res 28 (1995) 61.
[29] J.C. Hulteen, C.R. Martin, J. Mater. Chem. 7 (1997) 1075.
[30] C.R. Martin, Chem. Mater. 8 (1996) 1739.
[31] D. Routkevitch, T. Bigioni, M. Moskovits, J.M. Xu, J. Phys. Chem. 100 (1996) 14037.
[32] T.M. Whitney, J.S. Jiang, P.C. Searson, C.L. Chien, Science 261 (1993) 1316.
[33] F. Keller, M.S. Hunter, D.L. Robinson, J. Electrochem. Soc. 100 (1953) 411.
[34] Diggle, T.C. Downie, C.W. Goulding, Chem. Rev. 69 (1969) 365.
[35] H. Masuda, K. Fukuda, Science 268 (1995) 1466.
[36] H. Masuda, F. Hasegawa, S. Ono, J. Electrochem. Soc. 144 (1997) L127.
[37] O. Jessensky, F. Muller, U. Gosele, Appl. Phys. Lett. 72 (1998) 1173.
[38] A.P. Li, F. Muller, A. Birner, K. Nielsch, U. Gosele, J. Appl. Phys. 84 (1998) 6023.
[39] J.S. Suh, J.S. Lee, Appl. Phys. Lett. 75 (1999) 2047.
[40] M.J. Tierney, C.R. Martin, J. Phys. Chem. 93 (1989) 2878.
[41] C.J. Brumlik, C.R. Martin, J. Am. Chem. Soc. 113 (1991) 3174.
[42] C.J. Brumlik, C.R. Martin, K. Tokuda, Anal. Chem. 64 (1992) 1201.
[43] C.A. Foss Jr., G.L. Hornyak, J.A. Stockert, C.R. Martin, J. Phys. Chem. 96 (1992) 7497.
[44] C.A. Foss Jr., G.L. Hornyak, J.A. Stockert, C.R. Martin, Adv. Mater. 5 (1993) 135.
[45] C.A. Foss Jr., G.L. Hornyak, J.A. Stockert, C.R. Martin, J. Phys. Chem. 98 (1994) 2963.
[46] A.J. Yin, J. Li, W. Jian, A.J. Bennett, J.M. Xu, Appl. Phys. Lett. 79 (2001) 1039.
[47] P.C. Searson, R.C. Cammarata, C.L. Chien, J. Electron. Mater. 24 (1995) 955.
[48] G. Sauer, G. Brehm, S. Schneider, K. Nielsch, R.B. Wehrspohn, J. Choi, H. Hofmeister, U. Gosele, J. Appl. Phys. 91 (2002) 3243.
[49] Y.W. Wang, L.D. Zhang, G.W. Meng, X.S. Peng, Y.X. Jin, J. Zhang, J. Phys. Chem. B 106 (2002) 2502.
[50] L. Liang, J. Liu, C.F. Windisch, G.J. Exarhos, Y.H. Lin, Angew. Chem. Int. Ed. 41 (2002) 3665.
[51] S.A. Sapp, B.B. Lakshmi, C.R. Martin, Adv. Mater. 11 (1999) 402.
[52] J.D. Klein, R.D. Herrick, D. Palmer, M.J. Sailor, C.J. Brumlick, C.R. Martin, Chem. Mater. 5 (1993) 902.
[53] Y.J. Xu, D.S. Xu, D.P. Chen, G.L. Guo, C.J. Li, Acta Phys.-Chem. Sin. 15 (1999) 577.
[54] D.S. Xu, D.P. Chen, Y.J. Xu, X.S. Si, G.L. Guo, L.L. Gui, Y.Q. Tang, Pure Appl. Chem. 72 (2000) 127.
[55] D.S. Xu, Y.J. Xu, D.P. Chen, G.L. Guo, L.L. Gui, Y.Q. Tang, Chem. Phys. Lett. 325 (2000) 340.
[56] D.S. Xu, X.S. Si, G.L. Guo, L.L. Gui, Y.Q. Tang, J. Phys. Chem. B 104 (2000) 5061.
[57] D.S. Xu, Y.G. Guo, D.P. Yu, G.L. Guo, Y.Q. Tang, J. Mater. Res. 17 (2002) 1711.
[58] R.Z. Chen, D.S. Xu, G.L. Guo, Y.Q. Tang, J. Mater. Chem. 12 (2002) 2435.
[59] R.Z. Chen, D.S. Xu, G.L. Guo, L.L. Gui, Electrochem. Commun. 5 (2003) 579.
[60] X.S. Peng, G.W. Meng, J. Zhang, X.F. Wang, L.X. Zhao, Y.W. Wang, L.D. Zhang, Mater. Res. Bull. 37 (2001) 1369.
[61] X.S. Peng, G.W. Meng, J. Zhang, L.X. Zhao, X.F. Wang, Y.W. Wang, L.D. Zhang, J. Phys. D-Appl. Phys. 34 (2001) 3224.
[62] X.S. Peng, G.W. Meng, J. Zhang, X.F. Wang, X. Liu, L.D. Zhang, J. Mater. Res. 17 (2002) 1283.
[63] X.S. Peng, J. Zhang, X.F. Wang, Y.W. Wang, L.X. Zhao, G.W. Meng, L.D. Zhang, Chem. Phys. Lett. 343 (2001) 470.
[64] C.M. Shen, X.G. Zhang, H.L. Li, Mater. Sci. Eng. A 303 (2001) 19.
[65] R.Z. Chen, D.S. Xu, G.L. Guo, L.L. Gui, J. Electrochem. Soc. 150 (2003) G183.
[66] Y.J. Glanville, D.G. Narehood, P.E. Sokol, A. Amma, T. Mallouk, J. Mater. Chem. 12 (2002) 2433.
[67] A.L. Prieto, M.S. Sander, M.S. Martin-Gonzalez, R. Gronsky, T. Sands, A.M. Stacy, J. Am. Chem. Soc. 123 (2001) 7160.
[68] M.S. Sander, A.L. Prieto, R. Gronsky, T. Sands, A.M. Stacy, Adv. Mater. 14 (2002) 665.
[69] M.S. Sander, A.L. Prieto, R. Gronsky, T. Sands, A.M. Stacy, Chem. Mater. 15 (2003) 335.
[70] C.G. Jin, X.Q. Xiang, C. Jia, W.F. Liu, W.L. Cai, L.Z. Yao, X.G. Li, J. Phys. Chem. B 108 (2004) 1844.
[71] M.J. Zheng, L.D. Zhang, G.H. Li, W.Z. Shen, Chem. Phys. Lett. 363 (2002) 123.
[72] W.C. West, N.V. Myang, J.E. Whitacre, B.V. Ratnakumar, J. Power Sources 126 (2004) 203.
[73] K. Takahashi, S.J. Limmer, Y. Wang, G.Z. Cao, J. Phys. Chem. B 108 (2004) 9795.
[74] S. Kenane, L. Piraux, J. Mater. Res. 17 (2002) 401.
[75] D. Routkevitch, A.A. Tager, J. Haruyama, D. Almawlawi, M. Moskovits, J.M. Xu, IEEE Trans. Electron Devices 43 (1996) 1646.
[76] D. Routkevitch, T.L. Haslett, L. Ryan, T. Bigioni, C. Douketis, M. Moskovits, Chem. Phys. 210 (1996) 343.
[77] J.S. Suh, J.S. Lee, Chem. Phys. Lett. 281 (1997) 384.
[78] J.L. Hutchison, D. Routkevitch, M. Moskovits, R.R. Nayak, Inst. Phys. Conf. Ser. 157 (1997) 389.
[79] Y.Q. Liang, L. Zhai, X.S. Zhao, D.S. Xu, J. Phys. Chem. B 109 (2005) 7120.
[80] M. Martin-Gonzalez, G.J. Snyder, A.L. Prieto, R. Gronsky, T. Sands, A.M. Stacy, Nano Lett. 3 (2003) 973.
[81] M. Martin-Gonzalez, A.L. Prieto, R. Gronsky, T. Sands, A.M. Stacy, Adv. Mater. 15 (2003) 1003.
[82] D.S. Xu, Y.J. Xu, D.P. Chen, G.L. Guo, L.L. Gui, Y.Q. Tang, Adv. Mater. 12 (2000) 520.
[83] S.J. Limmer, S. Seraji, M.J. Forbess, Y. Wu, T.P. Chou, C. Nguyen, G.Z. Cao, Adv. Mater. 13 (2001) 1269.
[84] S.J. Limmer, S. Seraji, Y. Wu, M.J. Forbess, T.P. Chou, C. Nguyen, G.Z. Cao, Adv. Funct. Mater. 12 (2002) 59.
[85] S.J. Limmer, T.L. Hubler, G.Z. Cao, J. Sol–Gel Sci. Technol. 26 (2003) 577.
[86] Y.C. Wang, I.C. Leu, M.H. Hon, J. Mater. Chem. 12 (2002) 2439.
[87] Y.C. Wang, I.C. Leu, M.H. Hon, J. Cryst. Growth 237 (2002) 564.
[88] Y.C. Wang, I.C. Leu, M.H. Hon, Electrochem. Solid-State Lett. 5 (2002) C53.
[89] Y.G. Guo, C.J. Li, L.J. Wan, D.M. Chen, C.R. Wang, C.R. Bai, Y.G. Wang, Adv. Funct. Mater. 13 (2003) 626.
[90] Z. Miao, D.S. Xu, J.H. Ouyang, G.L. Guo, X.S. Zhao, Y.Q. Tang, Nano Lett. 2 (2002) 717.
[91] D.S. Xu, Y.X. Yu, Z. Miao, G.L. Guo, Y.Q. Tang, Electrochem. Commun. 5 (2003) 673.
[92] Y. Li, G.W. Meng, L.D. Zhang, F. Phillipp, Appl. Phys. Lett. 76 (2000) 2011.
[93] Y. Li, G.S. Cheng, L.D. Zhang, J. Mater. Res. 15 (2000) 2305.
[94] M.J. Zheng, G.H. Li, X.Y. Zhang, S.Y. Huang, Y. Lei, L.D. Zhang, Chem. Mater. 13 (2001) 3859.
[95] M.J. Zheng, L.D. Zhang, X.Y. Zhang, J. Zhang, G.H. Li, Chem. Phys. Lett. 334 (2001) 298.
[96] J.C. Fan, T. Gao, G.W. Meng, Y.W. Wang, X.N. Liu, L.D. Zhang, Mater. Lett. 57 (2002) 656.
[97] S. Tiwari, IEEE Electron Device Lett. 9 (1988) 142.
[98] B.B. Lakshmi, P.K. Dorhout, C.R. Martin, Chem. Mater. 9 (1997) 857.
[99] B.B. Lakshmi, C.J. Patrissi, C.R. Martin, Chem. Mater. 9 (1997) 2544.
[100] Y.K. Zhou, H.L. Li, J. Mater. Chem. 12 (2002) 681.
[101] B.A. Hernandez, K.S. Chang, E.R. Fisher, P.K. Dorhout, Chem. Mater. 14 (2002) 480.
[102] Y.K. Zhou, C.M. Shen, L.H. Li, Solid State Ionics 146 (2002) 81.
[103] M. Zhang, Y. Bando, K. Wada, J. Mater. Res. 16 (2001) 1408.
[104] C. Hippe, M. Wark, E. Lork, G. Schulz-Ekloff, Micropor. Mesopor. Mater. 31 (1999) 235.
[105] H.Q. Cao, Z. Xu, X.W. Wei, X. Ma, Z.L. Xue, Chem. Commun. 6 (2001) 541.
[106] C.T. Hsieh, J.M. Chen, H.H. Lin, H.C. Shih, Appl. Phys. Lett. 82 (2003) 3316.
[107] L.M. Huang, H.T. Wang, Z.B. Wang, A.P. Mitra, D. Zhao, Y.H. Yan, Chem. Mater. 14 (2002) 876.
[108] L.M. Huang, Z.B. Wang, H.T. Wang, X.L. Chen, A.P. Mitra, Y.H. Yan, J. Mater. Chem. 12 (2002) 388.
[109] L.M. Huang, H.T. Wang, Z.B. Wang, A. Mitra, K.N. Bozhilov, Y.S. Yan, Adv. Mater. 14 (2002) 61.
[110] L.F. Xu, Y. Guo, Q. Liao, J.P. Zhang, D.S. Xu, J. Phys. Chem. B 109 (2005) 13519.
[111] M.J. Siegfried, K.-S. Choi, Adv. Mater. 16 (2004) 1743.
[112] M.J. Siegfried, K.-S. Choi, Angew. Chem. Int. Ed. 44 (2005) 3218.
[113] M.J. Siegfried, K.-S. Choi, J. Am. Chem. Soc. 128 (2006) 10356.
[114] M.-P. Pileni, Nat. Mater. 2 (2003) 145.
[115] T. Pauprte, D. Lincot, Electrochim. Acta 45 (2000) 3345.
[116] R. Liu, A.A. Vertegel, E.W. Bohannan, T.A. Sorenson, J.A. Switzer, Chem. Mater. 13 (2001) 508.
[117] E. Jamil, T.Z. Ramon, L.C. Claude, J. Phys. Chem. C 112 (2008) 5736.
[118] J.H. Yang, G.M. Liu, J. Lu, Y.F. Qiu, S.H. Yang, Appl. Phys. Lett. 90 (2007) 103109.
[119] J.H. Yang, Y.F. Qiu, S.H. Yang, Cryst. Growth Des. 7 (2007) 2562.
[120] J. Hu, T.W. Odom, C.M. Liber, Acc. Chem. Res. 32 (1999) 435.
[121] S.B. Lee, D.T. Mitcell, L. Trofin, T.K. Nevanen, H. Soderlund, C.R. Martin, Science 296 (2002) 2198.
[122] J. Goldberger, R.R. He, Y.F. Zhang, S.K. Lee, H.Q. Yan, H.J. Choi, P.D. Yang, Nature 422 (2003) 599.
[123] L. Li, S.S. Pan, X.C. Dou, Y.G. Zhu, X.H. Huang, Y.W. Yang, G.H. Li, L.D. Zhang, J. Phys. Chem. C 111 (2007) 7288.
[124] J.C. Bao, C.Y. Tie, Z. Xu, Q.F. Zhou, D. Shen, Q. Ma, Adv. Mater. 13 (2001) 1631.
[125] W. Lee, R. Scholz, K. Nielsch, U. Gösele, Angew. Chem. Int. Ed. 44 (2005) 6050.

[126] C. Mu, Y.X. Yu, R.M. Wang, K. Wu, D.S. Xu, G.L. Guo, Adv. Mater. 16 (2004) 1550.
[127] C. Mu, Y.X. Yu, W. Liao, X.S. Zhao, D.S. Xu, Appl. Phys. Lett. 87 (2005) 113104.
[128] L.F. Xu, Q. Liao, J.P. Zhang, X.C. Ai, D.S. Xu, J. Phys. Chem. C 111 (2007) 4549.
[129] G.W. She, X.H. Zhang, W.S. Shi, X. Fan, J.C. Chang, Electrochem. Commun. 9 (2007) 2784.
[130] G.W. She, X.H. Zhang, W.S. Shi, X. Fan, J.C. Chang, C.S. Lee, S.T. Lee, C.H. Liu, Appl. Phys. Lett. 92 (2008) 053111.
[131] L.G. Yu, G.M. Zhang, S.Q. Li, Z.H. Xi, D.Z. Guo, J. Cryst. Growth 299 (2007) 184.
[132] Y.W. Tang, L.J. Luo, Z.J. Chen, Y. Jiang, B.H. Li, Z.Y. Jia, L. Xu, Electrochem. Commun. 9 (2007) 289.
[133] D. Gong, C.A. Grimes, O.K. Varghese, W.C. Hu, R.S. Singh, Z. Chen, E.C. Dickey, J. Mater. Res. 16 (2001) 3331.
[134] G.K. Mor, O.K. Varghese, M. Paulose, K. Shankar, C.A. Grimes, Solar Energy Mater. Solar Cells 90 (2006) 2011.
[135] J.M. Macak, H. Tsuchiya, L. Taveira, S. Aldabergerova, P. Schmuki, Angew. Chem. Int. Ed. 44 (2005) 7463.
[136] S. Yoriya, C.A. Grimes, Langmuir. doi:10.1021/la9020146.
[137] M. Paulose, K. Shankar, S. Yoriya, H.E. Prakasam, O.K. Varghese, G.K. Mor, T.A. Latempa, A. Fitzgerald, C.A. Grimes, J. Phys. Chem. B 110 (2006) 16179.
[138] S.P. Albu, A. Ghicov, J.M. Macak, P. Schmuki, Phys. Stat. Sol. (RRL) 1 (2007) R65.
[139] M. Paulose, H.E. Prakasam, O.K. Varghese, L. Peng, K.C. Popat, G.K. Mor, T.A. Desai, C.A. Grimes, J. Phys. Chem. C 111 (2007) 14993.
[140] S.P. Albu, A. Ghicov, S. Aldabergenova, P. Drechsel, D. Leclere, G.E. Thompson, J.M. Macak, P. Schmuki, Adv. Mater. 20 (2008) 4135.
[141] D. Kim, A. Ghicov, S.P. Albu, P. Schmuki, J. Am. Chem. Soc. 130 (2008) 16454.
[142] J.M. Macak, C. Zollfrank, B.J. Rodriguez, H. Tsuchiya, M. Alexe, P. Greil, P. Schmuki, Adv. Mater. 21 (2009) 3121.
[143] R. Hahn, F. Schmidt-Stein, J. Salonen, S. Thiemann, Y.Y. Song, J. Kunze, V.P. Lehto, P. Schmuki, Angew. Chem. Int. Ed. 48 (2009) 7236.
[144] S.P. Albu, A. Ghicov, J.M. Macak, R. Hahn, P. Schmuki, Nano Lett. 7 (2007) 1286.
[145] H.E. Prakasam, K. Shankar, M. Paulose, O.K. Varghese, C.A. Grimes, J. Phys. Chem. C 111 (2007) 7235.
[146] J. Wang, Z.Q. Lin, Chem. Mater. 20 (2008) 1257.
[147] J.H. Park, T.W. Leeb, M.G. Kang, Chem. Commun. 25 (2008) 2867.
[148] Q. Chen, D. Xu, Z. Wu, Z. Liu, Nanotechnology 19 (2008) 365708.
[149] Q. Chen, D. Xu, J. Phys. Chem. C 113 (2009) 6310.
[150] Z.R. Tian, J.A. Voigt, J. Liu, B. Mckenzie, M.J. Mcdermott, M.A. Rodriguez, H. Konishi, H. Xu, Nat. Mater. 2 (2003) 821.
[151] H.Q. Yan, R.R. He, J. Johnson, M. Law, R.J. Saykally, P.D. Yang, J. Am. Chem. Soc. 125 (2003) 4728.
[152] L. Manna, D.J. Milliron, A. Meisel, E.C. Scher, A.P. Alivisatos, Nat. Mater. 2 (2003) 382.
[153] Z.A. Peng, X.G. Peng, J. Am. Chem. Soc. 124 (2002) 3343.
[154] Z.L. Wang, X.Y. Kong, J.M. Zuo, Phys. Rev. Lett. 91 (2003) 185502.
[155] C. Ma, D. Moore, J. Li, Z.L. Wang, Adv. Mater. 15 (2003) 228.
[156] Z.L. Wang, Z.W. Pan, Adv. Mater. 14 (2002) 1029.
[157] P. Nguyue, H.T. Ng, J. Kong, A.M. Cassell, R. Quinn, J. Li, J. Han, M. McNeil, M. Meyyappan, Nano Lett. 3 (2003) 925.
[158] H.T. Shi, L.M. Qi, J.M. Ma, H.M. Cheng, J. Am. Chem. Soc. 125 (2003) 3450.
[159] T.L. Sounart, J. Liu, J.A. Voigt, J.W.P. Hsu, E.D. Spoerke, Z. Tian, Y.B. Jiang, Adv. Funct. Mater. 16 (2006) 335.
[160] M.J. Bierman, Y.K.A. Lau, A.V. Kvit, A.L. Schmitt, S. Jin, Science 320 (2008) 1060.
[161] J. Zhu, H. Peng, A.F. Marshall, D.M. Barnett, W.D. Nix, Y. Cui, Nat. Nanotechnol. 3 (2008) 477.
[162] L.F. Xu, Q.W. Chen, D.S. Xu, J. Phys. Chem. C 111 (2007) 11560.
[163] B.Q. Cao, X.M. Teng, S.H. Heo, Y. Li, S.O. Cho, G.H. Li, W.P. Cai, J. Phys. Chem. C 111 (2007) 2470.
[164] G.R. Li, X.H. Lu, D.L. Qu, C.Z. Yao, F.L. Zheng, Q. Bu, C.-R. Dawa, Y.X. Tong, J. Phys. Chem. C 111 (2007) 6678.
[165] M.S. Sander, H. Gao, J. Am. Chem. Soc. 127 (2005) 12158.
[166] A.S.M. Chong, L.K. Tan, J. Deng, H. Gao, Adv. Funct. Mater. 17 (2007) 1629.
[167] Y.Q. Liang, C.G. Zhen, D.C. Zou, D.S. Xu, J. Am. Chem. Soc. 126 (2004) 16338.
[168] L.E. Brus, J. Chem. Phys. 80 (1994) 4403.
[169] C.B. Murray, D.J. Norris, M.G. Bawendi, J. Am. Chem. Soc. 115 (1993) 8706.
[170] W.U. Huynh, J.J. Dittmer, A.P. Alivisatos, Science 295 (2002) 2425.
[171] K. Zhu, N.R. Neale, A. Miedaner, A.J. Frank, Nano Lett. 7 (2007) 69.
[172] J.R. Jennings, A. Ghicov, L.M. Peter, P. Schmuki, A.B. Walker, J. Am. Chem. Soc. 130 (2008) 13364.
[173] P. Roy, D. Kim, I. Paramasivam, P. Schmuki, Electrochem. Commun. 11 (2009) 1001.
[174] J.M. Macak, M. Zlamal, J. Krysa, P. Schmuki, Small 3 (2007) 300.
[175] I. Paramasivalm, J.M. Macak, P. Schmuki, Electrochem. Commun. 10 (2008) 71.
[176] M. Zlamal, J.M. Macak, P. Schmuki, J. Krysa, Electrochem. Commun. 9 (2007) 2822.
[177] G.K. Mor, K. Shankar, M. Paulose, O.K. Varghese, C.A. Grimes, Nano Lett. 5 (2005) 191.
[178] O.K. Varghese, M. Paulose, K. Shankar, G.K. Mor, C.A. Grimes, J. Nanosci. Nanotechnol. 5 (2005) 1158.
[179] M. Paulose, G.K. Mor, O.K. Varghese, K. Shankar, C.A. Grimes, J. Photochem. Photobiol. A 178 (2006) 8.